CLARA-A2: The second edition of the CM SAF cloud and radiation data record from 34 years of global AVHRR data

K.-G. Karlsson[1], K. Anttila[2], J. Trentmann[3], M. Stengel[3], J.F. Meirink[4], A. Devasthale[1], T. Hanschmann[3], S. Kothe[3], E. Jääskeläinen[2], J. Sedlar[1], N. Benas[4], G.-J. van Zadelhoff[4], C. Schlundt[3], D. Stein[3], S. Finkensieper[3], N. Håkansson[1] and R. Hollmann[3]

[1]{Swedish Meteorological and Hydrological Institute (SMHI), Norrköping, Sweden}

[2]{Finnish Meteorological Institute (FMI), Helsinki, Finland}

[3]{Deutscher Wetterdienst (DWD), Offenbach, Germany}

[4]{Royal Netherlands Meteorological Institute (KNMI), De Bilt, The Netherlands}

Correspondence to: K.-G. Karlsson (Karl-Goran.Karlsson@smhi.se)

Abstract

The second edition of the satellite-derived climate data record CLARA ("The CM SAF cLoud, Albedo and surface RAdiation dataset from AVHRR data" - second edition denoted CLARA-A2) is described. The data record covers the 34-year period from 1982 until 2015 and consists of cloud, surface albedo and surface radiation budget products derived from the AVHRR (Advanced Very High Resolution Radiometer) sensor carried by polar-orbiting, operational meteorological satellites. The data record is produced by the EUMETSAT Climate Monitoring Satellite Application Facility (CM SAF) project as part of the operational ground segment. Its upgraded content and methodology improvements since edition 1 are described in detail as well as some major validation results. Some of the main improvements of the data record come from a major effort in cleaning and homogenising the basic AVHRR level 1 radiance record and a systematic use of CALIPSO-CALIOP cloud information for development and validation purposes. Examples of applications studying decadal changes in Arctic summer surface albedo and cloud conditions, as well as global cloud redistribution patterns, are provided.

1 Introduction

Global distribution of cloudiness and existing cloud feedback on the radiative forcing continue to be important topics in climate research. Uncertainties in the description and understanding of both topics are considered to be dominant in explaining the spread among climate models in their prediction of current and anticipated climate change (Webb et al., 2013; Vial et al., 2013). In parallel, better knowledge and monitoring of global cloudiness

and radiation are also required for a successful increased utilisation of renewable energy sources, such as solar power plants (Šúri et al., 2007). In order to address requests and challenges in these and adjacent fields by a systematic utilization of satellite measurements, the Climate Monitoring Satellite Application Facility (CM SAF) was formed by the European Organisation for the Exploitation of Meteorological Satellites EUMETSAT (Schulz et al., 2009).

CM SAF (www.cmsaf.eu) aims at developing capabilities for a sustained generation and provision of Climate Data Records (CDRs) derived from operational meteorological satellites. The ultimate aim is to make the resulting data records suitable for the analysis of climate variability and the detection of climate trends. Examples of important guidelines for the compilation of CDRs are, (1) to apply the highest standards and guidelines as outlined by the Global Climate Observing System (GCOS), (2) to process satellite data within a true international collaboration benefiting from developments at international level and, (3) to perform intensive validation and improvement of the CM SAF CDRs, including a major role in data record assessments performed by research organizations such as the World Climate Research Programme (WCRP).

One of CM SAF's CDRs is CLARA: "The CM SAF cLoud, Albedo and surface RAdiation dataset from AVHRR data". It is based on data from the Advanced Very High Resolution Radiometer (AVHRR) operated onboard polar orbiting NOAA satellites as well as by the MetOp polar orbiters operated by EUMETSAT since 2006. AVHRR offers one of the longest satellite observation records, with its first measurements commencing in 1978. The first edition of CLARA (CLARA-A1) was released in 2012 and is described by Karlsson et al., (2013). This paper describes improvements and other features of the second edition, CLARA-A2, which was released in 2017.

The basic AVHRR radiance measurements were previously described in detail by Karlsson et al. (2013). Consequently, Section 2 describes only the extension of the data series since CLARA-A1 and some further modifications to improve calibration and homogenisation of the entire data record. Section 3 includes general descriptions on how the data record was compiled and Sections 4 through 6 explain the most significant improvements made to retrieval methods for the three different groups of parameters (clouds, surface albedo and radiation) together with some validation results. For the latter, some focus has been on extensive inter-comparisons being made to space-borne active lidar cloud retrievals (CALIPSO-CALIOP) and to other existing satellite-based data records (e.g., PATMOS-x and MODIS). Section 7 discusses potential applications and provides some examples of analyses possible from a continuous, homogeneous 34-yr data record. Finally, Section 8 summarises the main features of the data record and presents future plans.

2 Extension and homogenisation of the historic AVHRR data record

The basic AVHRR radiance measurements (level 1 observations) used in CLARA-A2 are described in detail by Karlsson et al. (2013). However, the temporal coverage is now extended with six additional years (2010-2015) resulting in a total length of 34 years (1982-2015). Figure 1 illustrates all satellites and their respective measurements periods for the CLARA-A2 climate data record. It is clear that the observational coverage varies considerably; there is only one satellite in orbit providing measurements during the 1980s and early 90s while during the last decade at least four simultaneous satellites were present (with a peak of 6 satellites available

simultaneously in 2009). Further, orbital drift for individual satellites leads to changing local observation times and this contributes to varying observational conditions during the period. However, some sub-setting of the data could still yield relatively homogeneous observation conditions. For example, choosing exclusively afternoon satellites (which is possible with the CLARA-A2 data record) a quite homogeneous and stable time series of observations can be achieved.

The AVHRR instrument was initially built for operational global weather monitoring purposes, not for climate monitoring. This means that the radiometric accuracy and the stability of radiance measurements are sometimes problematic for some early satellites in the time series. In addition, NOAA archiving of data has its own problems with intermittent occurrences of gaps, duplications and corrupt data, depending on time period and satellite. Consequently, a substantial effort in the preparation of CLARA-A2 has been made to correct and homogenize the entire radiance (level 1) record. A special pre-processing tool (PyGAC) was developed for these purposes, described in detail by Devasthale et al. (2016). Some of the most important aspects have been the following:

- Removal of corrupt data
- Data rescue of data with incorrect header definitions
- Removal of duplicated orbits
- Removal of overlap between orbits
- Homogenization of visible calibration by removal of trends and performing inter-calibration techniques between satellites (based on the method by Heidinger et al. (2010), but extended with more satellites and with MODIS Collection 6 as reference data)
- Improving accuracy of infrared calibration (compared to CLARA-A1) by using a more accurate treatment of calibration target data
- Applying median filters to AVHRR channel 3b (at 3.7 microns) brightness temperatures for reducing the impact of high noise levels for satellites NOAA-7 to NOAA-14
- Removal of partially corrupt orbits in periods with AVHRR scan motor problems (primarily between years 2001-2005; this was mostly based on manual inspection efforts since operational data flagging does not sufficiently cover this problem)

The overall impact of these treatments resulted in the exclusion of approximately 6 % of all original level 1 data in the NOAA archive from processing. The work with improving the AVHRR level 1 data record (or the Fundamental Climate Data Record – FCDR) has been performed within the framework of the WMO project SCOPE-CM (http://www.scope-cm.org/) and the ESA Cloud_cci project (http://www.esa-cloud_cci.org).

3 Product overview highlighting changes in product aggregation since CLARA-A1

The CLARA-A2 CDR is based on instantaneous AVHRR Global Area Coverage (GAC) retrievals (i.e., for every orbit at approximately 4 km horizontal swath resolution in nadir) which have been aggregated to derive the final spatio-temporally averaged data records. Since CLARA-A1, an important change for the cloud products is the introduction of globally resampled daily composites (level-2b) as the basis for computation of final level-3

products. The level-2b data representation (introduced by Heidinger et al., 2014) is motivated by the inhomogeneous global coverage of polar sun-synchronous satellite data. Each polar satellite offers around 14 evenly-distributed observations per day for each location near the poles, while at the equator, each location is observed only twice, approximately 12 hours apart. The purpose of the level-2b data representation is to form a more homogeneous data record having only two observations at the most nadir-viewing angle per day per satellite for each location globally. The alternative of using all available observations for Level-3 products (as was done for CLARA-A1) results in a skewed distribution of the observations because of the inhomogeneous observation frequency (increasing with latitude). By selecting only the observations which are made closest to the nadir condition, we ensure that observations are made at almost the same viewing conditions and, most importantly, observations are made at nearly the same local time globally for each level-2b product.

The level-2b approach leads to a significant reduction of the amount of used observations. However, the high observation frequency near the poles is undoubtedly very valuable, and, consequently, there are also separate polar products added which are based on all available observations. The level-2b approach is used exclusively for cloud products and not for surface radiation and surface albedo products where the use of all existing data is more critical.

Final level 3 cloud products are available as daily and monthly composites where the monthly means are computed from daily means. Results are defined for each satellite on a regular latitude/longitude grid with a spatial resolution of 0.25° × 0.25° degrees. In addition, results for cloud amount as well as the surface albedo (see Section 5) are available on two equal-area polar grids at 25 km resolution for the Arctic and Antarctic regions, respectively; these grids are centred at the poles and cover areas of approximately 9000 km x 9000 km. The new features for CLARA-A2 include the availability of all daily level-2b products and a demonstration data record of probabilistic cloud masks (further explained in the next section).

Monthly averages of cloud products are also available in aggregated form (i.e., merging all satellites). Acknowledging the different observation capabilities during night and during day, and also taking existing diurnal variations in cloudiness into consideration, a further separation of some products into exclusive day and night portions has been performed as a complement to the standard products based on all data. For these complementary products, all observations made under twilight conditions (solar zenith angles (SZA) between 75°-95°) have been excluded in order to avoid being affected by specific cloud detection problems occurring in the twilight zone (e.g. Derrien and LeGleau, 2010).

All products described in the following three sections are described in detail in Product User Manuals (PUM), Algorithm Theoretical Basis Documents (ATBD) and Validation reports (VAL), all available via the CM SAF web user interface (accessible from www.cmsaf.eu). These documents are important as they describe and reference the latest algorithms utilized in the processing of the CLARA-A2 data record; the peer-reviewed publications of retrieval algorithms referred to in the following Sections 4-6 may not always be up-to-date with these very latest algorithm changes.

4 Cloud products

A list of all CLARA-A2 aggregated cloud products is given in Tab. 1. These products have been derived from the pixel-level retrievals of the respective cloud properties, which are also made available in the form of level-2b products, as outlined in Section 3. Basic methods for deriving these parameters can be found in Karlsson et al. (2013). Consequently, the following sub-sections only provide a brief introduction to the products, list the most significant improvements since CLARA-A1 and introduce some new features.

4.1 Improvements of basic cloud products derived from the NWCSAF cloud processing package

The Cloud Fractional Cover (CFC) product is derived directly from results of a cloud screening, or cloud masking, method. CFC for one particular instantaneous observation is defined as the fraction of cloudy pixels per grid box compared to the total number of analysed pixels within that grid box, expressed as percent. This product is calculated using the NWC SAF Polar Platform System (PPS) cloud processing software (Dybbroe et al., 2005). CFC is also prepared in complementary daytime and nighttime conditions. The PPS method also computes the Cloud Top level (CTO) product, providing the cloud top level as geometric height, cloud top pressure and cloud top temperature. The CTO retrieval uses two different radiance matching methods, one for clouds identified as opaque and one for semi-transparent clouds.

CLARA-A2 takes advantage of some significant upgrades of the cloud masking and CTO retrievals in the latest PPS version. Generally, , the utilisation of reference measurements from the CALIPSO-CALIOP sensor (Winker et al., 2009, Vaughan et al., 2009) has been fundamental for the development and validation of the methods, following approaches by Karlsson and Dybbroe (2010) and Karlsson and Johansson (2013). The most important improvements regarding cloud screening include the following:

- PPS dynamic cloud masking thresholds have been adjusted,guided by cloud optical thickness information provided by CALIPSO-CALIOP, to detect a larger fraction of the thinnest clouds. Thus, thresholds for AVHRR visible reflectances and infrared brightness temperature differences (the latter often sensitive to presence of semi-transparent clouds) have been optimized.
- Identification of thin and fractional clouds over ocean surfaces has been improved by adding two new image feature tests: 1. Analysis of warmest pixels in a local neighbourhood. 2. Credibility tests of Sea Surface Temperature (SST) estimates based on standard SST retrieval schemes.
- New dynamic thresholds for infrared brightness temperature differences features have been introduced, in particular for the differences relative to the 3.7 micron channel over arid and semi-arid regions. For CLARA-A1 some static thresholds were used previously which led to occasional false cloudiness and unrealistic cloud distributions and trends over semi-arid regions as reported by Sun et al., (2015) and Sanchez-Lorenzo et. al., (2017). The new thresholds are functions of surface emissivity (from MODIS climatologies) and viewing angles. The impact of these changes is illustrated in Fig. 2 showing changes between CLARA-A1 and CLARA-A2 over the African continent. Clear reductions are shown over semi-arid regions while for other regions changes are close to neutral or slightly positive.

- The challenging cloud screening conditions near the poles have received special attention. Cloud detection during polar day conditions over snow- and ice-covered surfaces has been optimised and falsely detected clouds during polar night conditions have been largely removed. In both cases the access to CALIOP cloud masks and CALIOP-estimated cloud optical thicknesses has been extremely valuable. Various validation scores have been studied and PPS thresholds were adjusted to optimise the scores. The removal of falsely detected clouds unfortunately leads to a systematic and enhanced (compared to CLARA-A1) underestimation of cloudiness over the Arctic and Antarctic regions during polar night. However, we are of the opinion that this better reflects the true cloud detection limitations of the AVHRR sensor in situations with very cold ground temperatures compared to the previous case with frequently occurring false cloudiness.

Figure 3 compares results from CLARA-A1 and CLARA-A2 using global, synoptic surface observations (SYNOP) of cloud cover. For this study, the CLARA-A2 monthly mean product, generated from all available satellites, was compared against SYNOP monthly mean cloud cover calculated based on daily means. Only those stations and months where at least 6 observations per day for 20 days of the respective month were included in the comparison (see the VAL report for more details). Results show relatively small changes in CFC bias but a substantial decrease in the bias-corrected root mean squared error (bc-RMSE) for CLARA-A2. Thus, a much better agreement with the SYNOP observed variability in cloud cover is achieved. The relatively unchanged bias reflects inherent and unavoidable differences in the viewing geometry for the two observation types.

The improvements in cloud detection are also reflected in comparisons with cloud observations from the CALIPSO-CALIOP instrument. Karlsson and Johansson (2013) compared CLARA-A1 results with CALIPSO-CALIOP data for 99 selected NOAA-18 orbits and we have repeated this study for CLARA-A2 with overall global results provided in Tab. 2; the validation scores (bias, Kuipers and Hitrate) are explained in Karlsson and Johansson (2013). The number of matched field of views (FOVs) differs slightly here despite using the same 99 matched orbits which is explained by some pixels being masked out for quality reasons (in the polar areas) in the CLARA-A1 data record. We notice that more clouds are detected (bias being reduced) in CLARA-A2 despite the fact that some previous false classifications over semi-arid regions are now removed. Thus, both more clouds are detected and the cloudy/cloud-free separation has improved, indicated by improved Kuipers and Hitrate scores.

Figures 4 and 5 demonstrate the achievements made in cloud detection efficiency in CLARA-A2 in much more detail. Results are based on an extensive cloud product monitoring effort utilising near-simultaneous (i.e., within 3 minutes) observations from the CALIPSO-CALIOP sensor over nearly ten years (2006-2015). Despite the nadir-only observation capability of the CALIOP sensor compared to the wide-swath coverage from AVHRR, it has been possible to collect a global picture of cloud detection efficiency by accumulating results over the relatively long time period. Figure 4 shows the global overall frequency of correct cloudy and cloud-free estimations (Hitrate). In this figure we have only considered CALIOP-detected clouds with vertically integrated optical depths exceeding 0.15 (thinner clouds being treated as cloud-free cases). This is done to avoid being overly influenced by the presence of sub-visible clouds (explaining a large part of the negative bias values in Tab. 2) beyond detection capability in passive imagery. Results show a general global agreement in cloud screening well above 80 % apart from over the poles and high-latitude land areas and over high mountainous

terrain. Decreased Hitrates are also found over the marine sub-tropical regions near the climatological centres of sub-tropical highs. We suspect that this is mainly attributed to increasing geolocation mismatches between AVHRR- and CALIOP-observed clouds being present on the AVHRR GAC sub-pixel scale (less than 4 km). In other words, true small-scale or fractional clouds may exist in any of the two inter-compared data records but not always simultaneously in both because of the small sizes of cloud elements. These mismatches increase when facing conditions having a larger proportion of sub-AVHRR pixel scale cloudiness and such conditions are likely to occur in the central regions of the marine sub-tropical highs. Here we encounter more scattered cloudiness, occurring either as individual cumulus clouds or as broken stratocumulus or cumulus clouds in open cell formation (as described by Stevens et al., 2005) while away from these regions clouds organize more frequently as closed cells or as extensive stratocumulus cloud decks. Cases with a more dominant appearance of small cumulus and/or fractional stratocumulus can also occur over land surfaces but the more heterogenic conditions over land are likely to create a more diversified distribution of cumulus clouds in different stages of development and size. Nevertheless, the lower Hitrates also observed over the eastern part of South-America and in eastern Africa may also be explained by a high frequency of sub-pixel scale cloudiness.

The poorer results seen over regions where cold surface conditions may prevail for considerable portions of the year (Fig. 4) is a potentially more serious issue. Figure 5 exemplifies this by showing the probability of detecting cloudy conditions over the Arctic. Over the coldest portions of Greenland and the inner Arctic, almost 50 % of the clouds remain undetected in CLARA-A2 during the polar winter. On the other hand, cloud screening complications are reduced during the polar summer when results are nearly as good as over any other region on Earth (excluding some highly elevated areas of Greenland).

Comparisons have also been made to the MODIS (Moderate Resolution Imaging Spectroradiometer) sensor Collection 6 data record (http://modis-atmos.gsfc.nasa.gov/products_C006update.html) from the Aqua satellite (Fig. 6). Generally, we find a very good agreement between the two data records, both in the geographical distribution and in the zonal averages, of global cloud conditions for the overlapping data records of 2002-2014. There is a bias of about 5 % in cloud cover (MODIS higher) that is relatively constant over all latitudes (Fig. 6, lower panels). This increased cloudiness in MODIS is interpreted as representing the improvements in spectral channel availability of the MODIS sensor in comparison to AVHRR. However, the very good correlation with MODIS results is encouraging considering the availability of two more decades of results from AVHRR.

CLARA-A2 also includes a demonstration data record of probabilistic cloud masking following Karlsson et al. (2015), defined in the level 2b data record. The alternative formulation here provides a measure of uncertainty in cloud masking for the user to consult, compared to the traditional binary cloud mask utilized when compiling level 3 CFC products. The intention is to shift entirely to a probabilistic formulation in the third edition of CLARA planned for release in 2021.

The CTO retrieval in CLARA-A2 has been subject to several minor modifications while retaining the same principle methodology. However, the most significant improvement is related to an optimisation of the iterative procedure leading to a substantial efficiency leap regarding the fraction of resulting valid retrievals. The previous method in CLARA-A1 was not able to provide valid estimations for all semi-transparent clouds, where only approximately 70 % of all cloudy cases yielded valid CTO retrievals. The new PPS version used in CLARA-A2

processing provides CTO estimations for more than 97 % of all cases. This is especially important for the joint cloud-histogram product (JCH, see Section 3.3) and its ability to reflect true climatological conditions. The improvement has resulted from applying more physically sound constraints to the iterations (i.e., seeking the best physically reasonable solution instead of seeking the best solution and discarding it if it's not physically reasonable).

4.2 Cloud products derived from the CM SAF Cloud Physical Properties (CPP) package

The CPP products include cloud thermodynamic phase (CPH), cloud optical thickness (COT), particle effective radius (REF) and liquid/ice water path (LWP/IWP). Since 2012, the CPP package is included in the NWC SAF PPS cloud processing package. CPH is determined from a cloud typing approach following Pavolonis et al. (2005). This cloud type algorithm consists of a series of spectral tests applied to infrared brightness temperatures. It has a night-time branch, as well as a daytime branch in which shortwave reflectances are also considered. COT and REF are retrieved using the classical Nakajima and King (1990) approach, which is based on the principle that cloud reflectance is mainly dependent on COT at a non-absorbing, visible wavelength and on REF at an absorbing, near-infrared wavelength. In the CPP algorithm (Stengel et al., 2014; Roebeling et al., 2006), the Doubling-Adding KNMI (DAK, De Haan et al., 1987; Stammes, 2001) radiative transfer model is used to simulate visible (0.6 μm) and near-infrared (1.6/3.7 μm) TOA reflectances as a function of viewing geometry, COT, REF, and CPH. These simulated reflectances are stored in a look-up table (LUT) and satellite-observed reflectances are matched to this LUT in an iterative manner, leading to the derivation of COT and REF. These two parameters are then used to compute LWP and IWP, as in Stephens (1978). Uncertainty estimates of the CPP products are also derived and provided.

Major updates compared to the CPP version applied for CLARA-A1 (Karlsson et al., 2013) include the implementation of the new cloud phase algorithm in the NWC SAF PPS software package (first made in PPS version 2012 and for the latest improvements in PPS version 2014), the generation of improved cloud reflectance LUTs, and the inclusion of observational sea ice (OSI SAF, 2016) and ERA-Interim reanalysis (Dee et al., 2009) snow cover data to better characterize the surface albedo. It should be noted that, since CPP retrievals require reflectances from shortwave channels, CPP products, apart from CPH, are available exclusively during daytime (i.e., not during twilight and night). Since CPH is retrieved both during night and day, a complementary CPH(day) product is also provided.

Figure 7 shows the CPH, LWP and IWP products averaged over the 5-year period 2003-2007. Large scale climatological characteristics of clouds are apparent, including the marine stratocumulus regions off the west coasts of the continents, the Inter-Tropical Convergence Zone (ITCZ), consisting mainly of ice clouds, and the mid-latitude cyclone tracks in both hemispheres. High cloud water path values over polar regions should be largely attributed to inadequate retrievals over snow- and ice-covered surfaces, providing little contrast with clouds in the AVHRR visible channel.

Inter-comparison efforts with other similar data records show a general agreement better than 5 % for CPH (i.e, for absolute frequencies of water clouds) and 0.005 kg m^{-2} for LWP and IWP, although the bias compared to DARDAR IWP is larger. More details on these results can be found in the VAL report.

Further illustrations of LWP and IWP results are given in Figs 8 and 9. Figure 8a shows the monthly time series of LWP in the tropics from CLARA-A2, along with CLARA-A1 and two other satellite-based data records. Between them, PATMOS-x is the most similar to CLARA-A2, since it covers the same period and was based on the same (AVHRR) measurements. MODIS, on the other hand, covers the last 12 years of the time series and is the most stable, since it involves a single (here: MODIS on Aqua is used), well-calibrated instrument. In general, the LWP records agree well in terms of absolute amount of tropical LWP, except for a large bias in the case of CLARA-A1 (Fig. 8a). However, an improvement is apparent from CLARA-A1 to CLARA-A2, with the latter showing better agreement with PATMOS-x and MODIS. This difference between CLARA-A1 and CLARA-A2 is attributed mainly to changes in CPH, due to the implementation of a new retrieval algorithm. In terms of seasonal variability, all data records agree well, and differences between the two CLARA editions are minor (Fig. 8b). Both CLARA-A2 and PATMOS-x show some trends during various parts of the time series, which are primarily attributed to orbital drift.

It should also be noted that during the period 01/2001-05/2003, channel 3a of AVHRR onboard NOAA-16 was switched on and used for the retrievals, instead of channel 3b, which was used throughout the rest of the time series. This switch causes a jump in the time series of both CLARA-A2 and PATMOS-x. Comparisons of LWP were also made against an independent, microwave-based data record (O'Dell et al., 2008), focusing on the main stratocumulus regions, where liquid clouds prevail (not shown). Results showed good agreement in both the seasonal cycle and absolute values of LWP, with an average bias of -0.0034 kg m^{-2}, fluctuating in the range ±0.01 kg m^{-2}. Furthermore, Fig. 9 shows a validation of pixel-level CLARA-A2 IWP with Cloudsat-CALIOP-based DARDAR observations (Delanoë and Hogan, 2008). An overall underestimation by CLARA-A2 is observed, which becomes larger at high IWP values. Further analysis indicates that this disagreement is mainly caused by differences in REF (especially for thick clouds), while COT agrees well between the two data records (not shown).

4.3 Multi-parameter cloud product representations

The joint cloud property histogram (JCH) product is a combined histogram of CTP and COT covering the solution space of both parameters (e.g., Rossow and Schiffer, 1991). This two-dimensional histogram gives the frequency of occurrences for specific COT and CTP combinations defined by a constant bin space, separable for liquid and ice clouds. This product is defined on a slightly coarser grid (1°x1° resolution) in order to achieve higher statistical significance and to maintain manageable file sizes. The product is currently archived on the grid-point resolution, so user-defined JCH analysis regions can be created.

Since the JCH product is a product visualisation technique, its quality is dependent on the quality of the visualized products, including CTO (here, cloud top pressure), COT and CPH. Improvements of those products have already been described but we repeat some of the important points here:

- The increase in the number of valid CTO results gives a better representation of the true CTP-COT distribution
- The histograms are now based on cloud products defined in the level-2b representation mode giving a more homogeneous and consistent data distribution
- Frequencies of occurrences in each bin as well as the total cloud cover for all cases are now given (although the latter can still deviate slightly from the CFC product value since for JCH we require all three products - CTO, COT and CPH – to be simultaneously available).

Figure 10 shows global CLARA-A2 JCHs for afternoon satellites together with corresponding results from Aqua-MODIS Collection 6, PATMOS-x and CLARA-A1 over the period 2003-2014 (i.e., the Aqua-MODIS era). Notice, however, that there are no CLARA-A1 data after 2009 leading to a shorter period with data (2003-2009) for that data record in Fig. 10. In comparison to global JCH results for CLARA-A1 (Karlsson et al., 2013 and bottom panels in Fig. 10) we highlight that clouds are now more frequent at higher and lower tropospheric levels. This agrees well with MODIS and PATMOS-x, although the latter two have more boundary layer clouds present, especially over open water (Fig. 10d-i).

Over land, MODIS and PATMOS-x distributions show an increased frequency of mid- and high-level clouds, and a reduction in shallow cumulus and stratiform clouds (Fig. 10f, i). A relative increase in very optically thick mid- and upper-level clouds, representative of nimbostratus and deep convection, also emerges for MODIS and PATMOS-x. CLARA-A2 distributions generally agree with these distribution changes, although with CLARA-A2 there is a tendency to observe a higher frequency of optically thinner clouds (COT ranging 0.3-3.6) across the tropospheric column (Fig. 10c). Furthermore, there is a substantial amount of optically very thick mid- to upper-level clouds in CLARA-A2 and PATMOS-x (Fig. 10c, i), which are largely absent in MODIS (Fig. 10f). In CLARA-A2, this feature is linked to problems in estimating COT properly over snow-covered surfaces and therefore COT products over these surfaces should be treated with caution. A JCH where the Antarctic continent was masked resulted in the removal of this relative peak of high COT at mid- to high cloud levels in CLARA-A2 (not shown).

5 The surface albedo product

The cloud mask and AVHRR radiance data have been used as primary input data to generate the CLARA-A2 surface albedo (SAL) product of terrestrial black-sky surface albedo (wavelengths of 0.25-2.5 μm). It is available as pentad (five-day) and monthly means and has the same spatial resolution and projection as the other CLARA-A2 products. Examples of the CLARA-A2 SAL product for January and July 2012 are given in Fig. 11.

The retrieval algorithm of CLARA-A2 SAL follows the same outline as the previous CLARA-A1 SAL described in detail in Riihelä et al. (2013): After cloud masking, the possible effect of topography on geolocation and radiometry in locations with inclined slope is corrected. Then, for the pixels on land, a correction for scattering and absorption effects of aerosols and other atmospheric constituents is performed. In CLARA-A2 SAL, a dynamic aerosol optical depth (AOD) time series has been used. It has been composed using the Total Ozone Mapping Spectrometer (TOMS) and Ozone Monitoring Instrument (OMI) aerosol index data (Jääskeläinen et al., 2016). A correction for reflectance anisotropy of vegetated surfaces and spectral albedo is

then calculated. In CLARA-A1, one land use classification (LUC) was used for the whole time series. For the current SAL product, four different LUCs are used. Finally a narrow-to-broadband conversion is made to derive the albedo over the full spectral range of the product (0.25-2.5 μm). Since the reflectance anisotropy of snow is large and varies according to snow type (Peltoniemi et al., 2005), the albedo of snow and ice covered areas is derived by averaging the broadband bidirectional reflectances of the AVHRR overpasses into pentad or monthly means. These overpasses are found to cover the whole viewing hemisphere (SZA smaller than 70° and satellite zenith angles smaller than 60°) in most of the cases, giving a good representation of the bidirectional reflectance distribution function. For the observations over open water, the albedo is constructed as a function of SZA and wind speed. Wind information is taken from microwave measurements (SMMR and SSM/I data) and available SYNOP observations. The classification between open water and sea ice has been verified using the Ocean and Sea Ice Satellite Application Facility (OSI SAF) sea ice extent data (Eastwood, 2014).

In summary, the main differences in the algorithm between CLARA-A1 SAL and CLARA-A2 SAL are as follows:

- atmospheric correction uses dynamic AOD time series
- number of LUCs used has been increased from one to four
- wind speed data is used over sea to describe the sea surface roughness

The data record has been validated against in situ albedo observations from the Baseline Surface Radiation Network (Ohmura et al., 1998), the Greenland Climate Network (Steffen et al, 1996), and the TARA floating ice camp (Gascard et al., 2008). The sites have been chosen according to data availability, temporal coverage of measurements and quality of data. The validation results show that CLARA-A2 SAL has a relative accuracy of 10-20 % over vegetated sites, and typically 3-15 % over snow and ice. Larger differences between the in situ measurements and the satellite-based albedo value are mostly related to the heterogeneity of high-resolution near-infrared surface reflectances at CLARA-A2 SAL pixel scales. The spatial representativeness is an issue at most of the sites and should always be considered when using measurements of different scale (and location) for validation (Riihelä et al., 2012).

The SAL time series was also compared to MCD43C3, the surface albedo product from MODIS (Schaaf et al., 2002). The comparison showed that on a global scale, the two products are in good agreement. An overview of the MODIS comparison results for both CLARA-A2 and CLARA-A1 SAL can be seen in Fig. 12, showing the mean black sky albedo. These data have been averaged over the common retrievable land/snow area after coarsening the MODIS product to 0.25° spatial resolution and averaging the CLARA SAL pentad means to fit the MODIS products (delivered as 16-day means). Water areas are excluded from the analysis since the MODIS product is not defined for water bodies (including sea ice areas). The CLARA-A2 and MCD43C3 products are in good agreement and generally the albedo differences are less than 5 %, especially during the latter half of 2009. In general, the difference is caused by the methodology differences, where the MODIS albedo product is normalized to local noon, which, for surfaces other than snow, produces the minimum daily albedo. Taking this into consideration, CLARA-A2 SAL values are expected to be slightly higher than the MODIS product values. An analysis of the differences on latitudinal bands (not shown) shows that over the northern hemisphere, the largest differences appear over Arctic land areas. The topography (which is corrected for in SAL but not in the

MODIS product) also creates differences in the average albedo over mountainous regions. The albedo values of CLARA-A2 SAL are considerably closer to MODIS albedo values than CLARA-A1 SAL values are. This has been achieved by using dynamic AOD in the atmospheric correction of CLARA-A2 SAL.

The temporal stability of the CLARA-A2 SAL time series has also been evaluated using the central part of the Greenland ice sheet (not shown) as a site whose albedo is expected to remain fairly constant over a long period (Riihelä et al., 2013). The results showed that the maximum deviation of monthly mean CLARA-A2 SAL over this site from its 34-year mean was 8.5 %, including some natural variability associated with e.g. varying SZA. Also, the 34-year mean albedo for this site was estimated to be 0.786 which is somewhat lower than the literature citations for the albedo of dry fresh snow (0.85, Konzelmann and Ohmura, 1995).

The cloud mask used in CLARA-A2 SAL is less conservative than the one used in CLARA-A1 SAL. This is likely to affect the SAL values especially during non-continuous cloud conditions. Also the inaccuracies in the land cover data record used to resolve the CLARA-A2 SAL algorithms may cause retrieval errors. The users are recommended to utilize the existing support data (for example number of observations, standard deviation, mean SZA, skewness and kurtosis per pixel) to remove suspect retrievals from their analysis.

Our quality assessment of the CLARA-A1 SAL surface albedo data record has shown that SAL retrievals over snow and ice, particularly over the Arctic, are of good quality (Riihelä et al., 2010). Also, according to user feedback, the data record has been useful for climate model validation (e.g., Light et al., 2015). The retrieval over snow and ice is essentially the same in CLARA-A2 SAL as it was for the previous edition of the data record which gives reason to believe that the user feedback and quality assessment should, to some extent, also be valid for CLARA-A2. The validation results against in situ observations and comparison with MODIS MCD43C3 product show that adding the new AOD time series for land areas has improved the algorithm performance elsewhere as well.

6 Surface radiation products

The retrieval algorithms to derive the CLARA-A2 surface radiation products have only undergone minor changes since CLARA-A1. Details on the algorithms are given in Karlsson et al., (2013). Thus, this section presents a few validation results of the CLARA-A2 surface radiation data records.

6.1 Surface Solar Irradiance

The spatial data coverage of the surface solar irradiance (SIS) data has been substantially improved. In CLARA-A2, only snow-covered surfaces are excluded due to a reduced accuracy of the SIS data under these conditions. The validation against surface reference measurements from the Baseline Surface Radiation Network (BSRN) documents the improved accuracy of the CLARA A2 surface irradiance data record, mainly due to the improved cloud detection (see Tab. 3).

Figure 13 presents the comparison of the decadal linear trends derived from the CLARA-A2 SIS data record with the corresponding trends derived from measurements obtained from the BSRN. To assess the validity of the

linear trend derived from the CLARA data record, only surface stations with continuous observations covering at least 10 years of measurements are used.

The trends derived from the CLARA-A2 surface irradiance record correspond well to the trends derived from the BSRN measurements, indicating the high stability of the satellite-derived product and its suitability to calculate temporal changes and trends (Fig. 13). For most BSRN stations, the decadal trend is positive during the considered time period. Note that the time period for which BSRN measurements are available differs between the stations; consistent time periods were used to compare the CLARA-A2 SIS data record with the BSRN measurements at each station.

Figure 14 presents the spatial distribution of the decadal linear trend between 1992 and 2015 based on the CLARA-A2 SIS data record over Europe and a portion of Northern America. To limit the impact of the missing data during the first decade of the CLARA-A2 SIS data record due to the availability of only one AVHRR instrument, the trend was derived starting in 1992, when at least two AVHRR instruments have been available. In both regions there is an overall positive trend in surface irradiance, consistent with surface observations (e.g., Wild, 2012).

6.2 Surface Longwave Radiation

The CM SAF CLARA-A2 data record provides information on the surface longwave downwelling (SDL) and outgoing (SOL) radiation in order to enable studies of the full surface radiation budget. Both data records are dependent upon the surface longwave radiation records from the ERA-Interim reanalysis (Dee et al., 2009); using topographic information and the monthly mean cloud fraction from CLARA-A2, the ERA-Interim data are downscaled to match the spatial resolution of the CLARA–A2 data record. For SOL, this means a pure downscaling of ERA-Interim data. For SDL, an effective cloud factor is derived, based on ERA-Interim differences in clear-sky and all-sky downwelling longwave radiation, and reanalysis cloud fraction (Karlsson et al., 2013). This factor is then downscaled to CLARA-A2 resolution and multiplied by the CLARA-A2 satellite-derived cloud fraction. The result is a hybrid estimate of combined satellite-reanalysis SDL.

Table 4 shows the validation results of the monthly mean CLARA-A2 SOL and SDL data records compared to measurements obtained from the BSRN network. The improved cloud mask in CLARA-A2 led to a substantial improvement of the data quality of SDL data record relative to the CLARA-A1 data record.

7 Discussion: Demonstration of potential applications

The improvements of the underlying AVHRR radiance data record, the upgraded retrieval methods and the 6-year prolongation of the observation time series all increase the usefulness of the CLARA CDR for many applications. In other words, the potential for the data record to quantify true climate variability and trends has improved.

In this section, we wish to provide some exploratory results that can be directly derived from the new CLARA-A2 CDR, highlighting the potential value for different applications and future research directions.

The first example considers with the following question: How have surface and cloud conditions changed in the Arctic region over the last three to four decades? Similar studies on Arctic surface albedo variations alone have already been made based on CLARA-A1 data (Riihelä et al., 2013), but access to a longer time series of observations (including the new record year 2012 in Arctic minimum sea ice extent) and the coupling to cloud processes clearly motivate continued studies in this field. Many climate predictions and scenarios point towards the existence of an Arctic amplification (e.g., Cohen et al., 2014) of the regional temperature rise due to several large positive feedback effects; two of these effects are the decrease of sea ice cover and its interaction with cloudiness. The good AVHRR observation conditions during the polar summer season (e.g., as pointed out in Section 3.1 discussing Fig. 5) now permit more in depth studies of these two aspects.

Figure 15 shows the mean change of SAL for the first decade of the CLARA-A2 period (1982-1991) compared to the last decade (2006-2015) over the high-latitude Northern Hemisphere summer months. The corresponding changes in mean cloud cover are shown in Fig. 16. We can clearly see the strong SAL signal associated with Arctic sea ice decline since the 1980s, which is very evident in all months from May through September. Corresponding changes in Arctic cloudiness (Fig. 16) are, however, not as equally systematic and well depicted. This is not surprising since cloud conditions depend primarily on atmospheric circulation patterns. However, we notice a tendency for increased cloud cover over the marginal ice zone and the new ice-free regions of the inner Arctic in the months July-September while some decreases in cloud cover can be seen over the remaining ice-covered parts (e.g. close to Greenland and the Canadian archipelago). This result, based on long-term CLARA-A2 data, supports the findings by Devasthale et al. (2016) regarding a similar co-variability between cloudiness and sea-ice concentration observed in the last decade. An interesting feature in April-May is also the increase in cloud cover in the inner Arctic region while cloudiness appears to decrease outside of this area. However, further studies are needed to investigate the significance of these patterns and the possible links to changes in circulation and radiation conditions. For these purposes, the entire CLARA-A2 data record (i.e., including years 1992-2005) must be used.

Another example is related to studies of cloud-climate feedback processes which are known to explain a large part of the uncertainty in climate scenarios from model simulations. Norris et al. (2016) claim that we can already now see changes in global cloud patterns from long-term satellite observations, which are supported by climate model simulations. Specifically, the authors claim that there are signs of a decrease in mid-latitude cloudiness indicating “a poleward expansion of the subtropical dry zone cloud minimum and a poleward retreat of the storm-track cloud maximum”, based on a combined analysis of data from the ISCCP (Rossow and Schiffer, 1999) and PATMOS-x (Heidinger et al., 2104) climate data records covering the period 1983-2009. Similar changes in cloud patterns have been noticed in corresponding CMIP5 historical simulations (Norris et al., 2016).

Since CLARA-A2 is based on the same basic satellite radiance data record as PATMOS-x, and only differing in cloud retrieval methods, we could potentially see the same cloud changes. The CLARA-A2 availability of results for an additional 7 year period (with more stable satellite data less impacted by e.g., orbital drift effects) should also help giving some indication if the reported cloud change features remain or if they have changed in some way. Figure 17 shows the linear trend (note color scale is inverted relative to traditional depictions, where cold (warm) colors indicated positive (negative) cloud fraction trends), expressed as cloud fraction change over a 25-

year period but now estimated from 34 years of CLARA-A2 data, in comparison to only 27 years of data analysed by Norris et al. (2016). Comparisons with corresponding results by Norris et al. (2016) reveal many similarities, especially in the changed cloud distribution at low and tropical latitudes. It is apparent that in the latter part of the 34-year period we have had some dominance of strong El Nino events (e.g. 1997-1998 and 2015-2016) explaining the typical El Nino pattern over the central Pacific and Indonesia/Australia regions in Fig. 17. Interestingly, this signal is not as strong as in the study by Norris et al. (2016) which shows the value of studying a longer period where the ENSO extremes have a better chance of neutralizing each other in the long-term mean.

We notice that cloud distribution changes in other regions (e.g. the positive trends over Africa and in the eastern Pacific region) cannot be as clearly linked to typical El Nino Southern Oscillation (ENSO) patterns which is interesting. Whereas the agreement with Norris et al., (2016) is very good at low and tropical latitudes, the changes seen at mid- and high latitudes in the CLARA-A2 results are not as conclusive. There are some dominant negative trends over the typical extra-tropical storm track regions over the northern parts of the Atlantic and Pacific oceans but a similar change over the southern oceanic regions is not evident. We also see discrepancies over the eastern part of the Eurasian continent where CLARA-A2 shows a dominant decreasing trend. Based on these results we find it difficult to conclusively support the suggestions by Norris et al. (2016) regarding cloud changes at mid- and high-latitudes. If we consider the cloud trends derived from PATMOS-x and ISCCP separately (conclusions were drawn from a composited ISCCP-PATMOS-x data record), which were also provided by Norris et al. (2016), we find that mid-latitude trends for PATMOS-x show a better agreement with CLARA-A2 trends. This highlights the strength of data records comprised from polar-orbiting satellites, where better coverage of mid- and high-latitude regions is possible. Further studies are needed here to understand these differences.

A final remark regarding the use of CLARA-A2 results in climate model evaluation studies is that a COSP cloud observation simulator (Bodas-Salcedo et al., 2011) for CLARA-A2 is under preparation for facilitating comparisons with satellite-based results. In that way artefacts in the satellite observation and adequate corrections for viewing and observation conditions can be applied in order to give a more realistic inter-comparison of results between models and CLARA-A2 cloud products.

8 Summary and future plans

We have described the CLARA-A2 dataset – an improved 34-year cloud, surface albedo and radiation budget data record based on data from the AVHRR sensor on polar orbiting operational meteorological satellites. Major improvements in both the underlying AVHRR radiances and in the retrieval schemes have been described, together with some validation results. Regarding the latter, we have selected a limited glimpse at the exhaustive results created through the extensive validation efforts that have been conducted. More results and analyses are planned in follow-on papers. Some typical applications have also been demonstrated to encourage such studies using CLARA-A2 data records. We would also like to highlight the broadening of the CLARA portfolio of products which now also include daily aggregated and resampled orbits (level 2b) and the existence of an

experimental data record on probabilistic cloud masks. Related to this is the development of a CLARA-A2 cloud dataset COSP simulator.

A continuation of this work has recently been secured by the EUMETSAT approval of the third continuous operations and development phase (CDOP-3) of the CM SAF project covering the years 2017-2022. This means that a third edition of CLARA (CLARA-A3) is planned for release by the end of the CDOP-3 phase. This would be the last edition based entirely on original AVHRR data, including data from METOP-C (the last polar satellite carrying the AVHRR instrument). Furthermore, it will include an extension of the dataset with data forward in time for the years 2016-2020 and backward in time to 1978 (including data from the AVHRR/1 sensor starting with the Tiros-N satellite), which means it will cover more than 40 years in time. The product dataset will then also be extended with top of atmosphere radiation products and the original AVHRR radiances (level 1) will take advantage of a revised infrared calibration (following Mittaz and Harris, 2009), in addition to the upgraded visible calibration.

Appendix A: Acronym list

AOD	Aerosol Optical Depth
ATBD	Algorithm Theoretical Basis Document
AVHRR	Advanced Very High Resolution Radiometer (NOAA)
BSRN	Baseline Surface Radiation Network
CALIOP	Cloud-Aerosol Lidar with Orthogonal Polarisation (CALIPSO)
CALIPSO	Cloud-Aerosol Lidar and Infrared Pathfinder Satellite Observation satellite (NASA)
CDR	Climate Data Record
CERES	Clouds and the Earth's Radiant Energy System (NASA)
CFC	Cloud Fractional Cover product
CFMIP	Cloud Feedback Model Intercomparison Project
CLARA-A	The CM SAF cLoud, Albedo and surface RAdiation dataset from AVHRR data
CM SAF	Climate Monitoring Satellite Application Facility (EUMETSAT)
COSP	CFMIP Observation Simulation Package
COT	Cloud Optical Thickness product
CPH	Cloud Phase product
CPP	Cloud Physical Products package
CTO	Cloud TOp level product
DAK	Doubling-Adding KNMI radiative transfer model
ECMWF	European Centre for Medium-range Weather Forecasts
ENSO	El Nino Southern Oscillation
ERA-Interim	ECMWF ReAnalysis Interim dataset
EUMETSAT	EUropean organisation for exploitation of METeorological SATellites
FCDR	Fundamental Climate Data Record
GAC	Global Area Coverage (AVHRR, 5 km global resolution)
GCOS	Global Climate Observing System (WMO)
GEWEX	Global Energy and Water cycle EXperiment

ISCCP	International Satellite Cloud Climatology Project
ITCZ	Inter-Tropical Convergence Zone
IWP	Ice Water Path product
JCH	Joint Cloud property Histograms
LUC	Land Use Classification
LUT	Look Up Table
LWP	Liquid Water Path product
MCD43C3	MODerate-resolution Imaging Spectroradiometer (MODIS) Albedo product
MODIS	Moderate Resolution Imaging Spectroradiometer (NASA)
NASA	National Aeronautics and Space Administration (USA)
NOAA	National Oceanographic and Atmospheric Administration (USA)
NWCSAF	Nowcasting Satellite Application Facility (EUMETSAT)
PATMOS-x	The AVHRR Pathfinder Atmospheres Extended dataset (NOAA)
PPS	Polar Platform Systems package (EUMETSAT, NWCSAF)
PUM	Product User Manual
PyGAC	Python module for AVHRR GAC pre-processing
REFF	Cloud Effective Radius product
SAL	Surface ALbedo product
SMMR	Scanning Multichannel Microwave Radiometer (Nimbus 7 satellite)
SSM/I	Special Sensor Microwave Imager
	(Defense Meteorological Satellite Program – DMSP – satellites)
SYNOP	Synoptical weather observations from surface stations
TOA	Top Of Atmosphere
VAL	VALidation report
WCRP	World Climate Research Programme
WMO	World Meteorological Organisation

Acknowledgements

The authors want to thank Dr. Andrew Heidinger at NOAA for providing the method for inter-calibrating historic visible AVHRR radiances. CALIPSO-CALIOP datasets were obtained from the NASA Langley Research Center Atmospheric Science Data Center Surface meteorological and Solar Energy (SSE) web portal supported by the NASA LaRC POWER Project.

This work is funded by EUMETSAT in cooperation with the national meteorological institutes of Germany, Sweden, Finland, the Netherlands, Belgium, Switzerland and United Kingdom.

The CLARA-A2 data record is (as all CM SAF CDRs) freely available via the website https://www.cmsaf.eu.

References

Bodas-Salcedo, A., Webb, M.J., Bony, S., Chepfer, H., Dufresne, J.-L., Klein, S.A., Zhang, Y., Marchand, R., Haynes, J.M., Pincus, R. and John, V.O.: COSP: Satellite simulation software for model assessment, Bull. Amer. Meteor. Soc., August 2011, 1023-1043, doi: 10.1175/2011BAMS2856.1 , 2011.

Cohen, J., Screen, J.A., Furtado, J.C., Barlow, M., Whittleston, D., Coumou, D., Francis, J., Dethloff, K., Entekhabi, D., Overland, J. and Jones, J.: Recent Arctic amplification and extreme mid-latitude weather. Nature Geoscience, 7, 627-637, doi:10.1038/ngeo2234, 2014.

Dee, D. P., Uppala, S. M., Simmons, A. J., Berrisford, P., Poli, P., Kobayashi, S., Andrae, U., Balmaseda, M. A., Balsamo, G., Bauer, P., Bechtold, P., Beljaars, A. C. M., van de Berg, L., Bidlot, J., Bormann, N., Delsol, C., Dragani, R., Fuentes, M., Geer, A. J., Haimberger, L., Healy, S. B., Hersbach, H., Hólm, E. V., Isaksen, L., Kållberg, P., Köhler, M., Matricardi, M., McNally, A. P., Monge-Sanz, B. M., Morcrette, J.-J., Park, B.-K., Peubey, C., de Rosnay, P., Tavolato, C., Thépaut, J.-N., Vitart, F.: The ERA-Interim reanalysis: configuration and performance of the data assimilation system, Quarterly Journal of the Royal Meteorological Society, 137, 656, (doi = 10.1002/qj.828), 553—597, 2011.

De Haan, J. F., Bosma, P. and Hovenier, J.W.: The adding method for multiple scattering calculations of polarized light, Astron. Astrophys., 183, 371-391, 1987.

Delanoë, J., and R. J. Hogan: A variational scheme for retrieving ice cloud properties from combined radar, lidar, and infrared radiometer, J. Geophys. Res., 113, D07204, doi:10.1029/2007JD009000, 2008.

Derrien, M. and LeGleau, H.: Improvement of cloud detection near sunrise and sunset by temporal-differencing and region-growing techniques with real-time SEVIRI, Int. J. Remote Sens., 31, 1765-1780, DOI:10.1080/01431160902926632, 2010.

Devasthale, A., J. Sedlar, B. Kahn, M. Tjernström, E. Fetzer, B. Tian, J. Teixeira, and T. Pagano: A decade of space borne observations of the Arctic atmosphere: novel insights from NASA's Atmospheric Infrared Sounder (AIRS) instrument. Bull. Amer. Meteor. Soc. doi:10.1175/BAMS-D-14-00202.1, 2016 (in press). http://journals.ametsoc.org/doi/pdf/10.1175/BAMS-D-14-00202.1

Devasthale, A., Raspaud, M., Schlundt, C., Hanschmann, T., Finkensieper, S., Dybbroe, A., Hörnquist, S., Håkansson, N., Stengel, M. and Karlsson, K.-G.: PyGAC: an open-source, community-driven Python interface to preprocess more than 30-year AVHRR Global Area Coverage (GAC) data. 2016 (in preparation).

Dybbroe, A., Thoss, A. and Karlsson, K.-G.: NWCSAF AVHRR cloud detection and analysis using dynamic thresholds and radiative transfer modelling – Part I: Algorithm description, J. Appl. Meteor, 44, 39-54, 2005.

Eastwood, S.: Sea Ice Product User's Manual OSI-401-a, OSI-402-a, OSI-403-a. Version 3.11. September 2014, http://osisaf.met.no/docs/osisaf_ss2_pum_ice-conc-edge-type.pdf, doi: 10.15770/EUM_SAF_OSI_0005 (https://www.researchgate.net/publication/294892033_OSI_SAF_global_sea_ice_concentration_data_record_-_OSI-409a)

Gascard, J.-C., Bruemmer, B., Offermann, M., Doble, M., Wadhams, P., Forsberg, R., Hanson, S., Skourup, H., Gerland, S., Nicolaus, M., Metaxian, J.-P., Grangeon, J., Haapala, J., Rinne, E., Haas, C., Heygster, G., Jakobson, E., Palo, T., Wilkinson, J., Kaleschke, L., Claffey, K., Elder, B., and Bottenheim, J.: Exploring Arctic Transpolar Drift During Dramatic Sea Ice Retreat, EOS, 89, 21–28, 2008.

Heidinger, A.K., Straka, W.C., Molling, C.C., Sullivan, J.T. and Wu, X.Q.: Deriving an inter-sensor consistent calibration for the AVHRR solar reflectance data record. Int. J. Rem. Sens., 31(24), 6493-6517, 2010.

Heidinger, A. K., Foster, M. J., Walther, A. & Zhao, Z.: The Pathfinder Atmospheres Extended (PATMOS-x) AVHRR climate data set. Bull. Am. Meteorol. Soc. 95, 909–922, 2014.

Jääskeläinen, E., Manninen, T., Tamminen, J. and Laine, M.: An Aerosol Optical Depth time series 1982-2014 for atmospheric correction from OMI and TOMS Aerosol Index, Atmospheric Measurement Techniques Discussion, doi:10.5194/amt-2016-180, 2016 (in preparation).

Karlsson K.-G. and A. Dybbroe: Evaluation of Arctic cloud products from the EUMETSAT Climate Monitoring Satellite Application Facility based on CALIPSO-CALIOP observations. Atmos. Chem. Phys., 10, 1789–1807, 2010.

Karlsson, K.-G. and E. Johansson: On the optimal method for evaluating cloud products from passive satellite imagery using CALIPSO-CALIOP data: example investigating the CM SAF CLARA-A1 dataset. Atmos. Meas. Tech., 6, 1271–1286, www.atmos-meas-tech.net/6/1271/2013/ , doi:10.5194/amt-6-1271-2013, 2013.

Karlsson, K.-G., E. Johansson and A. Devasthale: Advancing the uncertainty characterisation of cloud masking in passive satellite imagery: Probabilistic formulations for NOAA AVHRR data, Rem. Sens. Env. , 158, 126-139; doi:10.1016/j.rse.2014.10.028, 2015.

Karlsson, K.-G., Riihelä, A., Müller, R., Meirink, J. F., Sedlar, J., Stengel, M., Lockhoff, M., Trentmann, J., Kaspar, F., Hollmann, R., and Wolters, E.: CLARA-A1: a cloud, albedo, and radiation dataset from 28 yr of global AVHRR data, Atmos. Chem. Phys., 13, 5351-5367, doi:10.5194/acp-13-5351-2013, 2013.

Konzelmann, T. and Ohmura, A.: Radiative fluxes and their impact on the energy balance of the Greenland Ice Sheet, Journal of Glaciology, 41, 490–502, 1995.

Light, B., S. Dickinson, D. K. Perovich, and M. M. Holland: Evolution of summer Arctic sea ice albedo in CCSM4 simulations: Episodic summer snowfall and frozen summers, J. Geophys. Res. Ocean., 120(1), 1–20, doi:10.1002/2014JC010149, 2015.

Mittaz, P.D. and Harris, R.: A Physical Method for the Calibration of the AVHRR/3 Thermal IR Channels 1:The Prelaunch Calibration Data.J. Atmos.Ocean. Tech., 26, 996-1019, doi: 10.1175/2008JTECHO636.1, 2009.

Nakajima, T., and M. D. King: Determination of the Optical Thickness and Effective Particle Radius of Clouds from Reflected Solar Radiation Measurements. Part 1: Theory. J. Atmos. Sci ., 47, 1878-1893, 1990.

Norris, J. R. , R. J. Allen, A. T. Evan, M. D. Zelinka, C. W. O'Dell & Stephen A. Klein: Evidence for climate change in the satellite cloud record, Nature 536, 72–75 (04 August 2016), doi:10.1038/nature18273, 2016.

O'Dell, C.W., Wentz, F.J. and Bennartz, R.: Cloud Liquid Water Path from Satellite-Based Passive Microwave Observations: A New Climatology over the Global Oceans. J. Climate, 21, 1721–1739, doi:10.1175/2007JCLI1958.1, 2008.

OSI SAF: The EUMETSAT OSI SAF Sea Ice Concentration Algorithm. Algorithm Theoretical Basis Document, SAF/OSI/CDOP/DMI/SCI/MA/189, Version 1.5, 2016.

Ohmura, A., Gilgen, H., Hegner, H., Müller, G., Wild, M., Dutton, E. G., Forgan, B., Fröhlich, C., Philipona, R., Heimo, A., König-Langlo, G., McArthur, B., Pinker, R., Whitlock, C. H., and Dehne, K.: Baseline Surface Radiation Network (BSRN/WCRP): New Precision Radiometry for Climate Research., Bulletin of the American Meteorological Society, 79, 2115–2136, doi:10.1175/1520-0477(1998)079h2115: BSRNBWi2.0.CO;2, 1998.

Pavolonis, M. J., Heidinger, A. K., and Uttal, T.: Daytime global cloud typing from AVHRR and VIIRS: Algorithm description, validation, and comparison, J. Appl. Meteorol., 44, 804-826, doi:10.1175/JAM2236.1, 2005.

Peltoniemi, J.I.; Kaasalainen, S.; Naranen, J.; Matikainen, L.; Piironen, J.: Measurement of directional and spectral signatures of light reflectance by snow. IEEE Transactions on Geoscience and Remote Sensing, 43 (10), 2294- 2304, 2005.

Riihelä A., Laine V., Manninen T., Palo T., Vihma T.: Validation of the CM SAF surface broadband albedo product: Comparisons with in situ observations over Greenland and the ice-covered Arctic Ocean. Remote Sensing of Environment, 114 (11), 2779-2790, 2010.

Riihelä, A., Manninen, T. and Laine, V.: Observed changes in the albedo of the Arctic sea-ice zone for the period 1982-2009, Nature Climate Change, 3, 895-898, doi:10.1038/nclimate1963, 2013.

Riihelä, A., Manninen, T., Laine, V., Andersson, K., and Kaspar, F.: CLARA-SAL: a global 28-yr timeseries of Earth's black-sky surface albedo, Atmos. Chem. Phys. , 13, 3743-3762, doi:10.5194/acp-13-3743-2013, 2013.

Roebeling, R. A., A. J. Feijt, A.J. and Stammes, P.: Cloud property retrievals for climate monitoring: implications of differences between SEVIRI on METEOSAT-8 and AVHRR on NOAA-17, J. Geophys. Res., 111, D20210, doi:10.1029/2005JD006990, 2006.

Rossow, W. B. and Schiffer, R. A.: ISCCP Cloud Data Products. Bull. Am. Meteorol. Soc. 72, 2-20, doi: 10.1175/1520-0477(1991)072<0002:ICDP>2.0.CO;2, 1991.

Rossow, W. B. and Schiffer, R. A.: Advances in understanding clouds from ISCCP. Bull. Am. Meteorol. Soc. 80, 2261–2287, 1999.

Sanchez-Lorenzo, A., A. Enriquez-Alonso, J. Calbó, J.-A. González, M. Wild, D. Folini, J. R. Norris and S. M. Vicente-Serrano: Fewer clouds in the Mediterranean: consistency of observations and climate simulations. Nature Scientific Reports 7, doi:10.1038/srep41475, 2017.

Schaaf, C.B., Gao, F., Strahler, A.H., Lucht, W., Lia,X., Tsang, T., Strugnell, N.C., Zhang, X., Jin, Y., Muller, J.-P., Lewis, P., Barnsley, M., Hobson, P., Disney, M., Roberts, G., Dunderdale, M., Doll, C., d'Entremont, R.P.,

Hu, B., Liang, S., Privette, J.L. and Royh, D.: First operational BRDF, albedo nadir reflectance products from MODIS, Remote Sens. Environ., 83, 2002.

Schulz, J., Albert, P., Behr, H.-D., Caprion, D., Deneke, H., Dewitte, S., Dürr, B., Fuchs, P., Gratzki, A., Hechler, P., Hollmann, R., Johnston, S., Karlsson, K.-G., Manninen, T., Müller, R., Reuter, M., Riihelä, A., Roebeling, R., Selbach, N., Tetzlaff, A., Thomas, W., Werscheck, M., Wolters, E., and Zelenka, A.: Operational climate monitoring from space: the EUMETSAT Satellite Application Facility on Climate Monitoring (CM-SAF), Atmos. Chem. Phys., 9, 1687-1709, doi: 10.5194/acp-9-1687-2009, 2009.

Stammes, P.: Spectral radiance modelling in the UV-Visible range. IRS 2000: Current problems in Atmospheric Radiation, edited by W.L. Smith and Y.M. Timofeyev, pp 385-388, A. Deepak Publ., Hampton, VA, 2001.

Stengel, M., A. Kniffka, J.F. Meirink, M. Lockhoff, J. Tan and R. Hollmann, CLAAS: the CM SAF cloud property dataset using SEVIRI, Atm. Chem. Phys., 14, 4297-4311, doi:10.5194/acp-14-4297-2014, 2014.

Stengel, M., S. Mieruch, M. Jerg, K.G. Karlsson, R. Scheirer, B. Maddux, J.F. Meirink, C. Poulsen, R. Siddans, A. Walther and R. Hollmann, The Clouds Climate Change Initiative: Assessment of state-of-the-art cloud property retrieval schemes applied to AVHRR heritage measurements, Remote Sens. Environ., doi:10.1016/j.rse.2013.10.035, 2013.

Stephens, G.: Radiation profiles in extended water clouds. II: Parameterization schemes. J. Atmos. Sci., 35, 2123-2132, 1978.

Steffen, K., Box, J., and Abdalati, W.: Greenland Climate Network: GC-Net, CRREL 96-27 Special Report on Glaciers, Ice Sheets and Volcanoes, tribute to M. Meier, pp. 98–103, 1996.

Stevens, B., Vali, G., Comstock, K., Wood, R., van Zanten, M. C., Austin, P. H., Bretherton, C. S. and Lenschow, D. H.: Pockets of open cells and drizzle in marina stratocumulus, Bull. Amer. Met. Soc., January 2005, 51-57, 2005.

Sun, B., Free,M., Yoo, H. L., Foster, M. J., Heidinger, A. and Karlsson, K.-G.: Variability and Trends in US Cloud Cover: ISCCP, PATMOS-x and CLARA-A1 Compared to Homogeneity-Adjusted Weather Observations, J. Climate, June 2015, DOI: http://dx.doi.org/10.1175/JCLI-D-14-00805.1, 2015.

Šúri, M., Huld, T.A., Dunlop, E.D. and Ossenbrink, H.A.: Potential of solar electricity generation in the European Union member states and candidate countries. Solar Energy, 81, 1295-1305, doi:10.1016/j.solener.2006.12.007, 2007.

Vaughan, M., Powell, K., Kuehn, Rl.,Young, S., Winker, D., Hostetler, C., Hunt, W., Liu, Z., McGill, M., and Getzewich, B.: Fully Automated Detection of Cloud and Aerosol Layers in the CALIPSO Lidar Measurements, J. Atmos. Oceanic Technol., 26, 2034–2050, doi: 10.1175/2009JTECHA1228.1, 2009.

Vial, J., Dufresne, J.-L. & Bony, S. On the interpretation of inter-model spread in CMIP5 climate sensitivity estimates. Clim. Dyn. 41, 3339–3362, 2013.

Webb, M. J., Lambert, F. H. & Gregory, J. M. Origins of differences in climate sensitivity, forcing and feedback in climate models. Clim. Dyn. 40, 677–707, 2013.

Wild, M.: Enlightening global dimming and brightening, Bull. Amer. Meteor. Soc., January 2012, 27-37, http://dx.doi.org/10.1175/BAMS-D-11-00074.1, 2012.

Winker, D. M., Vaughan, M.A., Omar, A., Hu, Y, Powell, K.A., Liu, Z., Hunt, W.H., and Young, S.A.: Overview of the CALIPSO mission and CALIOP data processing algorithms, J. Atmos. Oceanic. Technol., 26, 2310-2323, doi:10.1175/2009JTECHA1281.1, 2009.

Table 1: CLARA-A2 level 3 cloud products.

Product identifier	Product name	Description
CFC	Cloud Fractional Cover	Average fraction (%) of cloudy pixels in grid point.
CTO	Cloud Top level	Cloud top defined in one of three options: geometrical height (m), pressure (hPa) or brightness temperature (K).
CPH	Cloud phase	Average fraction (%) of liquid water cloud pixels relative to all cloudy pixels. Product defined both day and night (new feature compared to CLARA-A1).
COT	Cloud Optical Thickness	Average (both linear and logarithmic) of cloud optical thickness for liquid and ice clouds separately (dimensionless).
REF	Cloud Effective Radius	Average of cloud particle sizes for liquid and ice clouds separately (μm).
LWP	Liquid Water Path	Average (in-cloud and all-sky) of column integrated liquid water (kgm^{-2}).
IWP	Ice Water Path	Average (in-cloud and all-sky) of column integrated frozen water (kgm^{-2}).
JCH	Joint Cloud Histogram	2-D histograms of occurrences in predefined cloud top pressure – cloud optical thickness bins. Defined for both water and ice clouds in a 1° x 1° geographical grid. Only valid for daytime conditions (see text for further explanation).

Table 2: Globally averaged validation results of the CLARA-A2 and CLARA-A1 cloud detection (cloud mask) compared to CALIPSO-CALIOP observations based on 99 reference NOAA-18 and CALIPSO orbits in the period October 2006 to December 2009. Shown are the number of matched field of views (FOVs) and the validation scores mean error (bias), Kuipers and Hitrate.

Data record	# FOVs	Bias (%)	Kuipers	Hitrate (%)
CLARA-A2	787 102	-13.2	0.64	79.7
CLARA-A1	725 900	-14.4	0.56	75.8

Table 3: Validation results of the CLARA-A2 surface irradiance (SIS) data record (monthly mean / daily mean) against the global data from the BSRN network; for reference the corresponding values for CLARA-A1 are also given. Shown are the number of months/days, the bias and the absolute bias as well as the correlation of the anomaly between the two CLARA data records and the BSRN data.

Data record	# obs	Bias (W/m^2)	Abs. bias (W/m^2)	Corr. Ano
CLARA-A2	6420 / 181649	-1.6 / -1.7	8.8 / 27.7	0.87 / 0.90
CLARA-A1	3105 / 96237	-3.3 / - 4.7	10.4 / 34.3	0.88 / 0.85

Table 4: Validation results of the monthly mean CLARA-A2 SOL and SDL data records compared to the measurements from the BSRN network. As references also the results obtained from CLARA-A1 and ERA-Interim are shown. Presented are the number of months used for the ccomparison, the bias and the absolute bias, as well as the correlation of the anomalies.

Data record	# Months	Bias (W/m^2)	Abs. bias (W/m^2)	Corr. Ano
SOL (A2/A1/ERA-I)	1680 / 1270 / 1680	2.9 / 5.8 / 1.9	13.7 / 13.8 / 14.1	0.74 / 0.71 / 0.78
SDL (A2/A1/ERA-I)	7302 / 5314 / 7302	-4.7 / -3.7 / -6.4	7.9 / 8.3 / 9.4	0.84 / 0.82 / 0.84

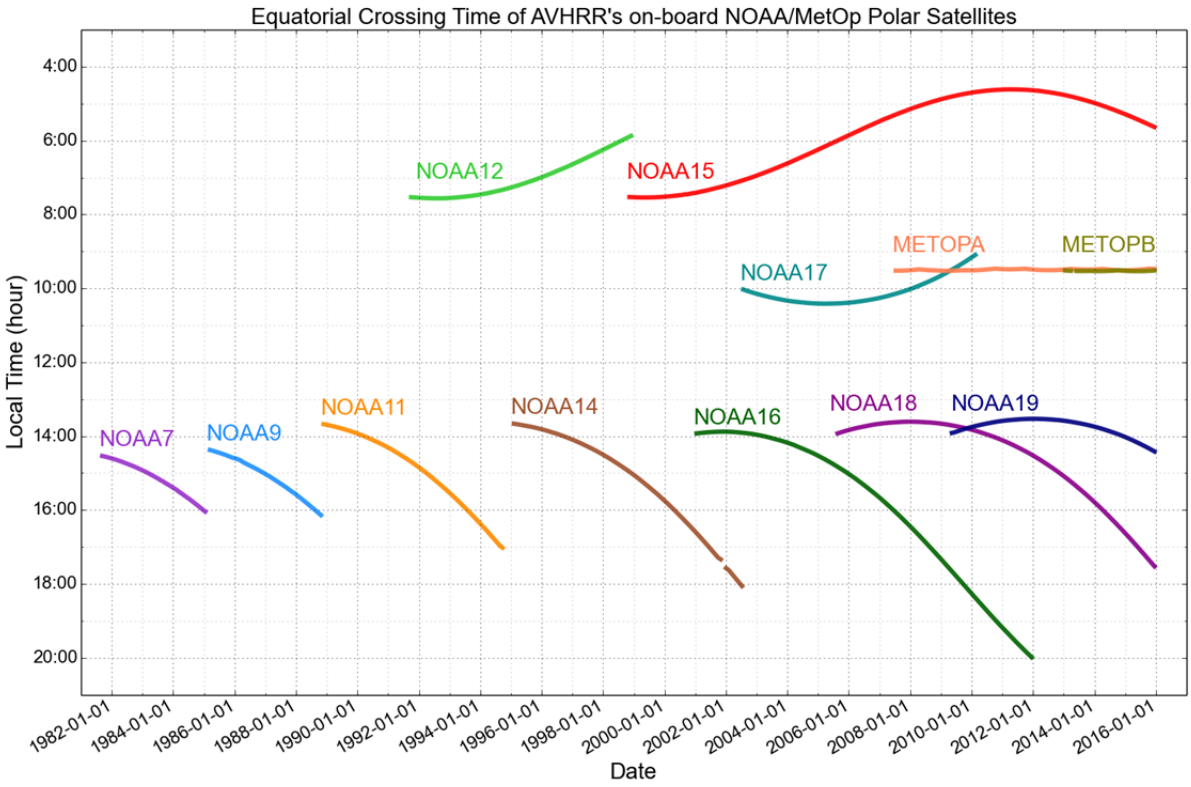

Figure 1: Daytime equator observation times for all satellites covered by CLARA-A2 from NOAA-7 to NOAA-19 and METOP A/B. The figure shows ascending (northbound) equator crossing times for all afternoon satellites fromNOAA-7 to NOAA-19 and descending (southbound) equator crossing times for all morning satellites (NOAA-12, NOAA-15NOAA-17 and METOP A+B). Corresponding night-time or evening observations take place 12 hours earlier/later. Some data gaps are present but only for a number of isolated dates.

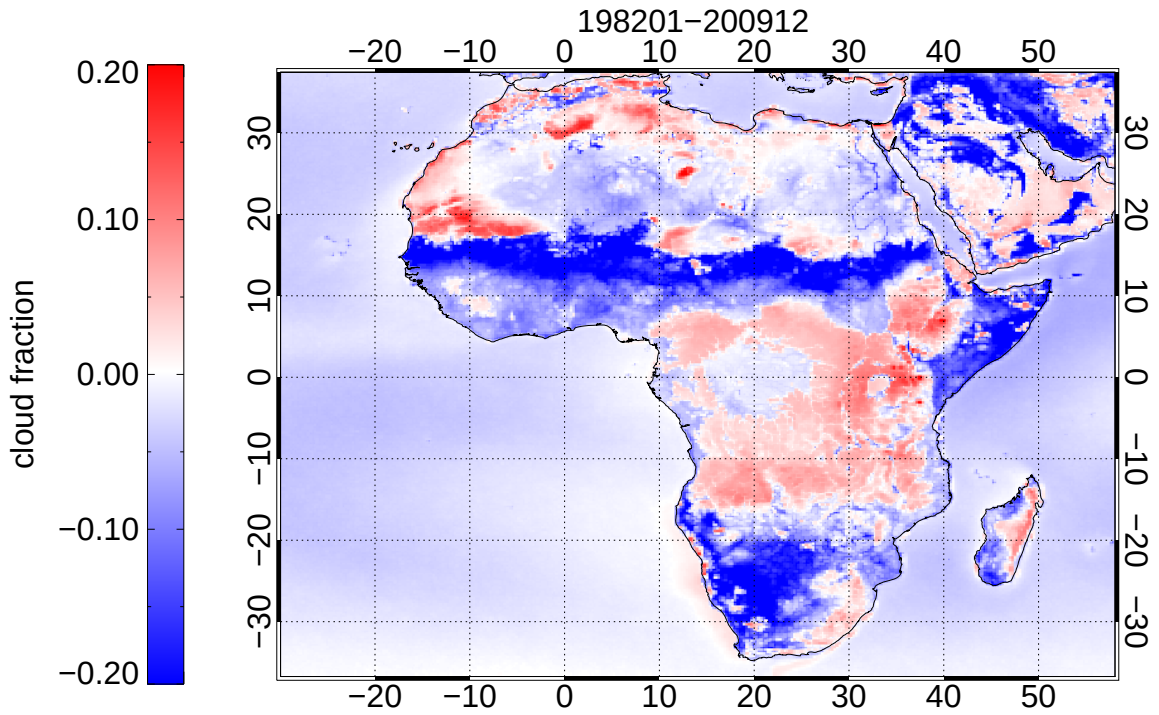

Figure 2: Mean difference in cloud fraction between CLARA-A2 and CLARA-A1 for the common period 1982-2009 over the African continent.

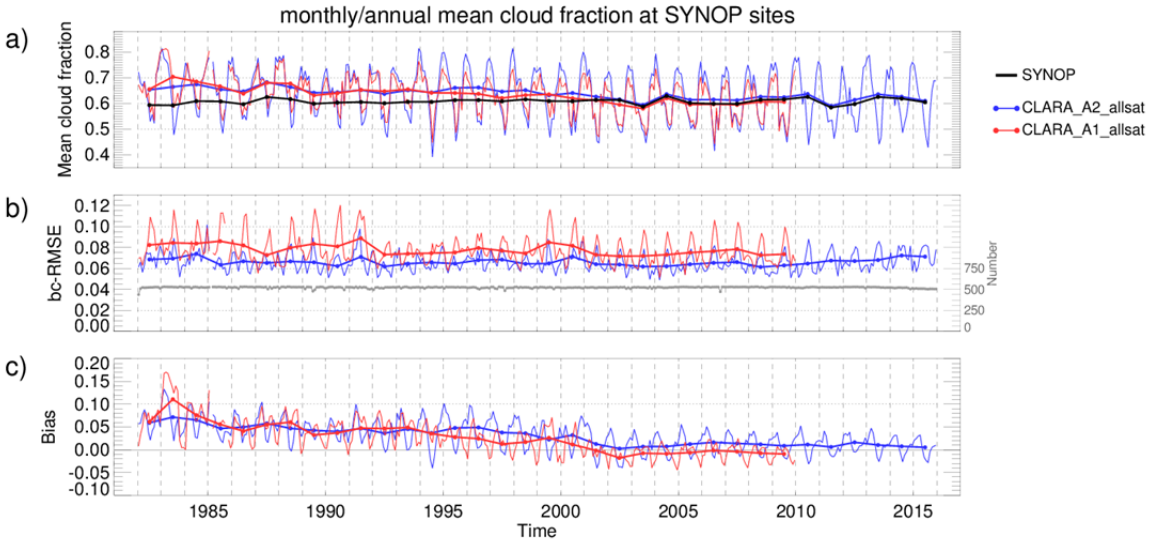

Figure 3: (a) Time series of mean monthly and annual cloud fraction for CLARA-A2 (blue), CLARA-A1 (red), and SYNOP (black), (b) bias-corrected RMSE and (c) bias for the entire period 1982-2015. See text for further details.

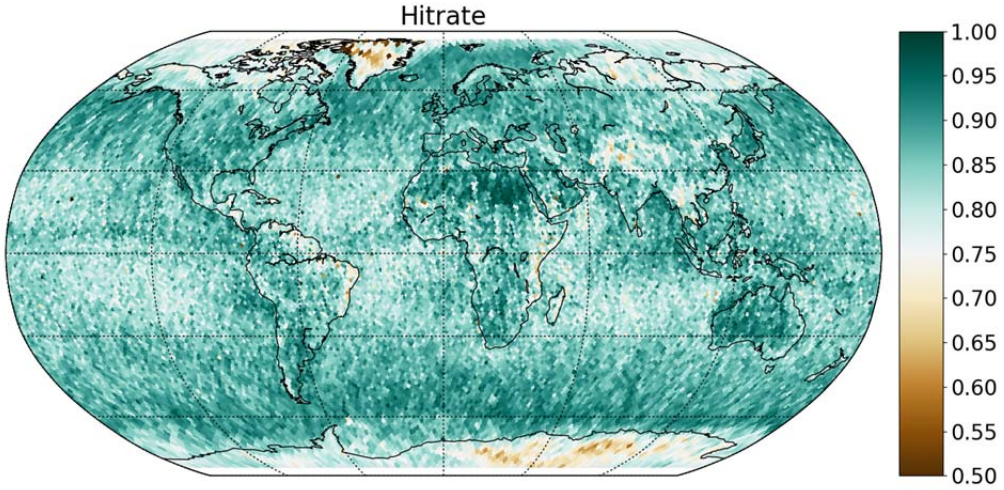

Figure 4: Global overall frequency of correct cloudy and cloud-free estimations (often referred to as the Hitrate) derived from nearly 10 000 collocated (within 3 minutes) near-nadir AVHRR and CALIPSO-CALIOP orbits in the period 2006-2015. The Hitrate was calculated after discarding CALIOP-detected clouds with cloud optical thicknesses below 0.15. Results are collected in a Fibonacci grid with 28878 grid points evenly spread out around the Earth approximately 150 km apart. The resulting grid has almost equal area and almost equal shape of all grid cells. White spots are cells with insufficient coverage of collocations.

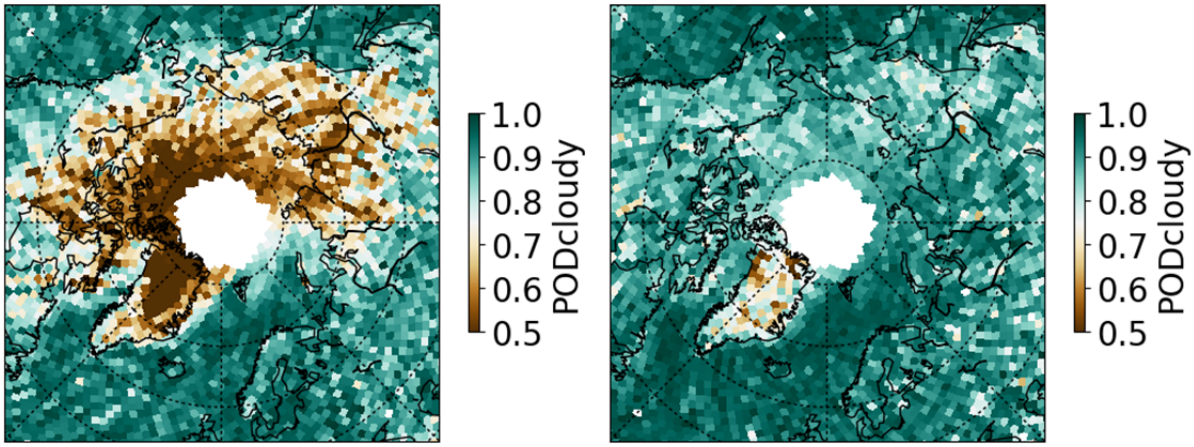

Figure 5: Probability of detecting cloudy conditions over the Arctic region during the polar winter (left) and during the polar summer (right). Results were derived from the same dataset as in Fig. 3.

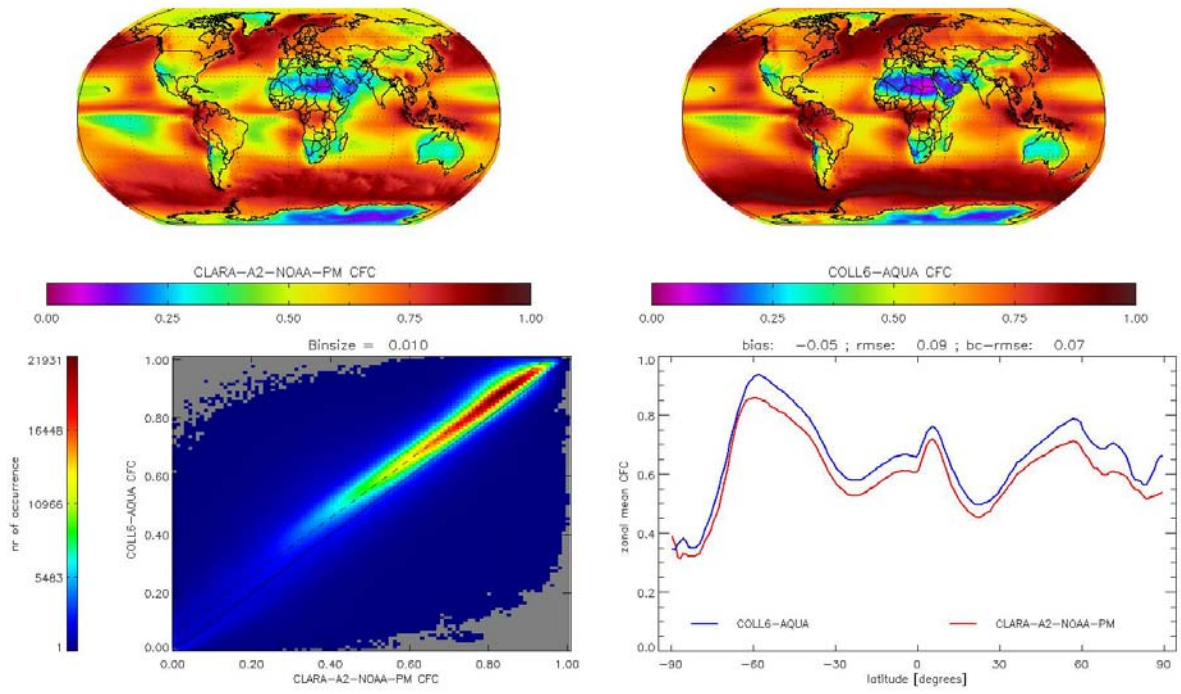

Figure 6: Intercomparison of CLARA-A2 and MODIS Collection 6 (Aqua part) cloud fraction over the covered MODIS period 2002-2014. Upper left: CLARA-A2 global cloud cover (CFC). Upper right: MODIS global cloud cover. Lower left: Scatterplot of the two data records. Lower right: Latitudinal distribution (zonal means) of cloud cover from the two data records (CLARA –A2 in red and MODIS in blue).

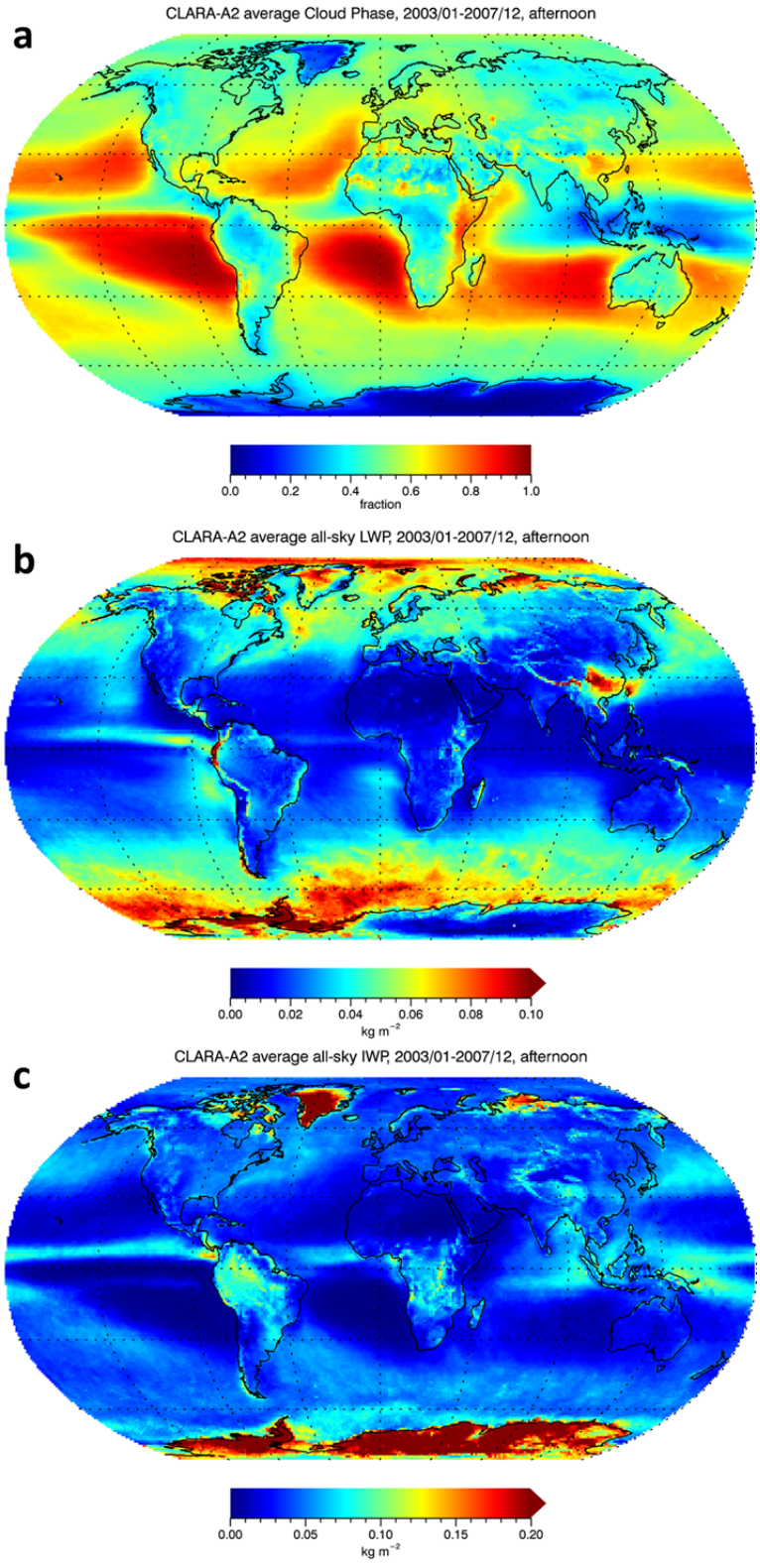

Figure 7: (a) Fraction of liquid clouds relative to total cloud fraction, (b) all-sky liquid water path and (c) all-sky ice water path, averaged for the 5-year period 2003-2007. All data come from CLARA-A2 level 3 products, derived from afternoon (NOAA-16 and NOAA-18) satellite measurements. Water paths in kg m^2.

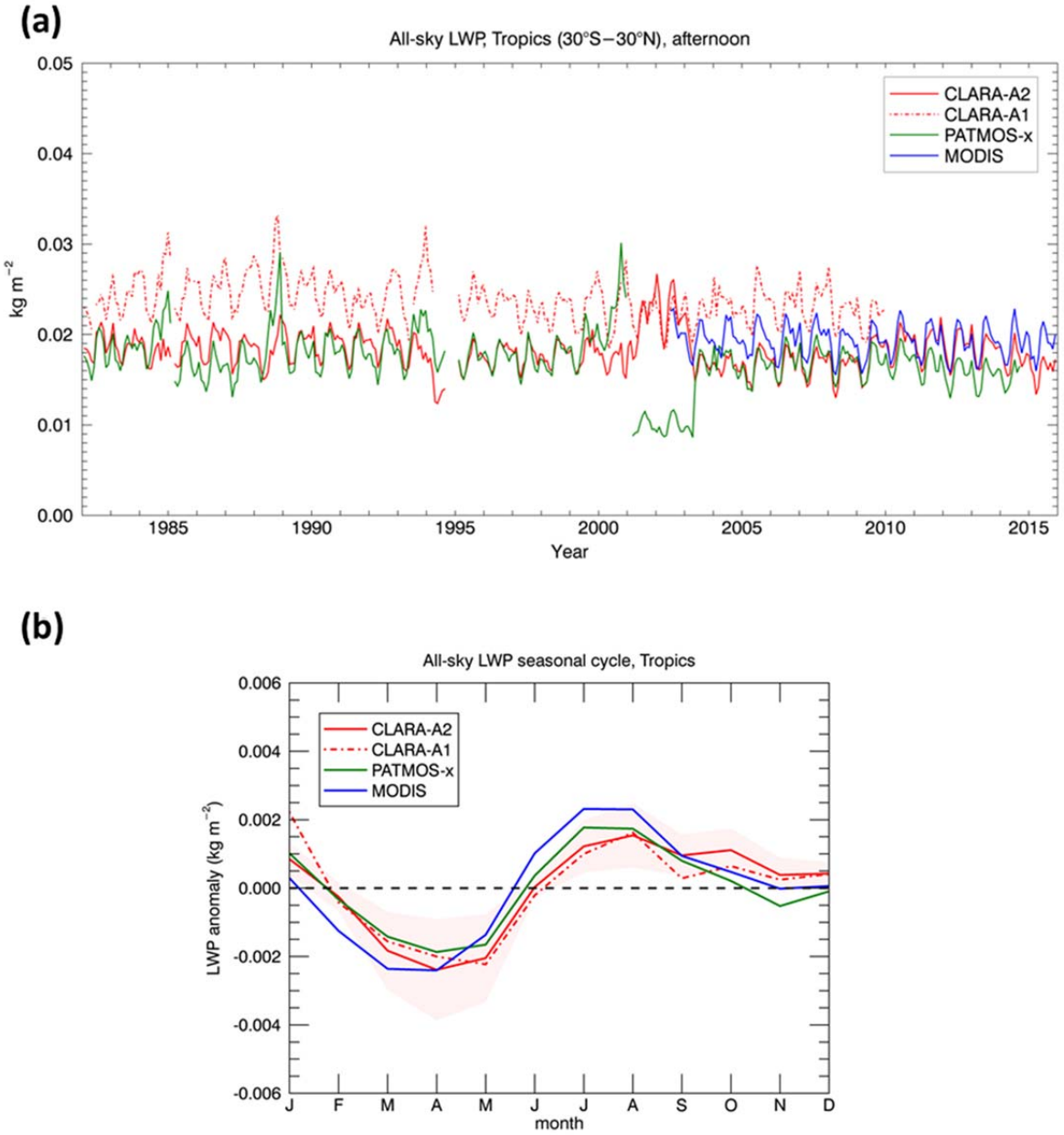

Figure 8: Comparison between CLARA-A2, CLARA-A1, PATMOS-x and MODIS all-sky liquid water path (kgm^{-2}) for the Tropics (30°S – 30°N): monthly time series (top) and seasonal anomaly (bottom). The seasonal anomaly is calculated as the average of the deviations of monthly means from the corresponding yearly mean over the years 2003-2009. The shaded area around the CLARA-A2 curve indicates +/- 1 standard deviation of these deviations. The plots have been compiled from the NOAA afternoon satellites (NOAA-7, -9, -11, -14, -16, -18, and -19) for CLARA-A2, CLARA-A1 and PATMOS-x, and the MODIS Aqua (MYD08 Collection 6) 3.7 µm product.

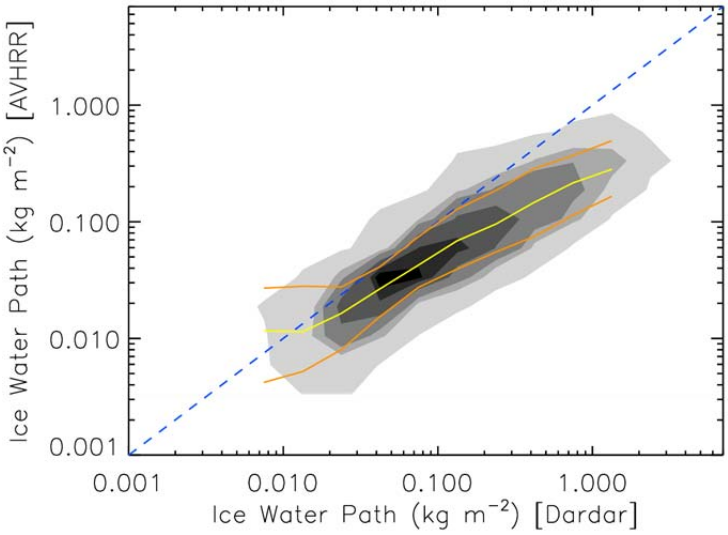

Figure 9: CLARA-A2 (NOAA-18) IWP vs. DARDAR IWP (kg m^{-2}) for the months January and July 2008. The yellow line depicts the median and orange lines the 16th/84th percentiles of the CLARA-A2 distribution at the corresponding DARDAR IWP. The greyscales indicate regions enclosing the 10, 20, 40, 60, and 75% of points with the highest occurrence frequency.

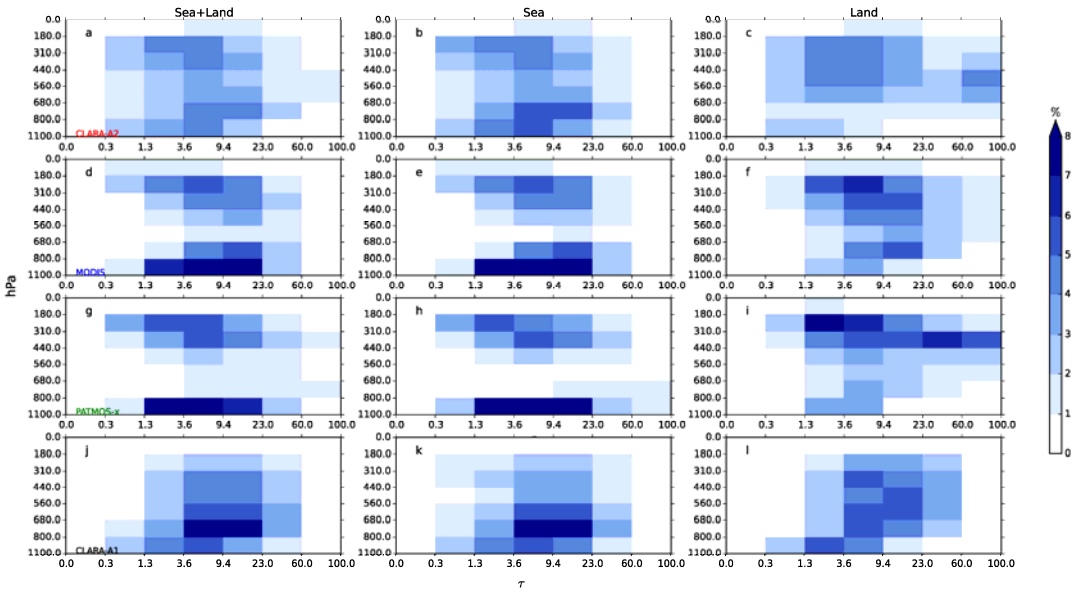

Figure 10: Global JCH relative frequency distributions [colors, %] of CTP [hPa] and COT for all months for four data records: CLARA-A2 (panels a-c), MODIS Collection 6 (panels d-f), PATMOS-X (panels g-i) and CLARA-A1 (panels j-l).. The covered period is 2003-2013 except for CLARA-A1 which only covers the period 2003-2009 (no data after 2009). Left column contains the JCHs over sea and land surfaces (sea+land), middle column over sea-only surfaces (sea) and right column over land-only surfaces (land). Histogram frequencies are normalized to unity, such that each histogram sums to 100%.

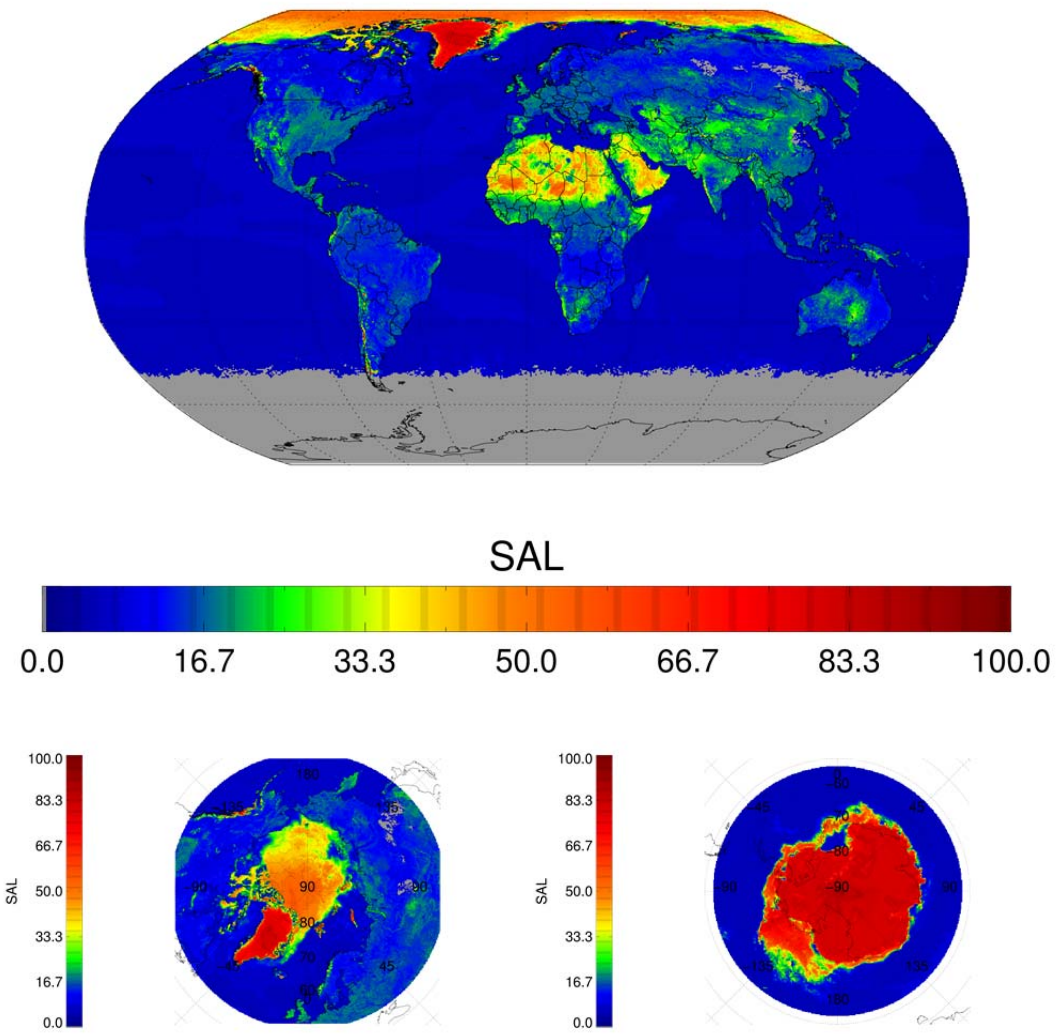

Figure 11: Global monthly mean surface albedo for July 2012 (top). Corresponding plots for two polar grids are shown at the bottom of the figure; one for the Arctic region (bottom left) and one for the Antarctic region (bottom right, but observe that the month here is January instead of July). Regions without values are grey-shaded (here resulting from dark conditions prevailing close to Antarctica during the polar winter). All albedos given as %.

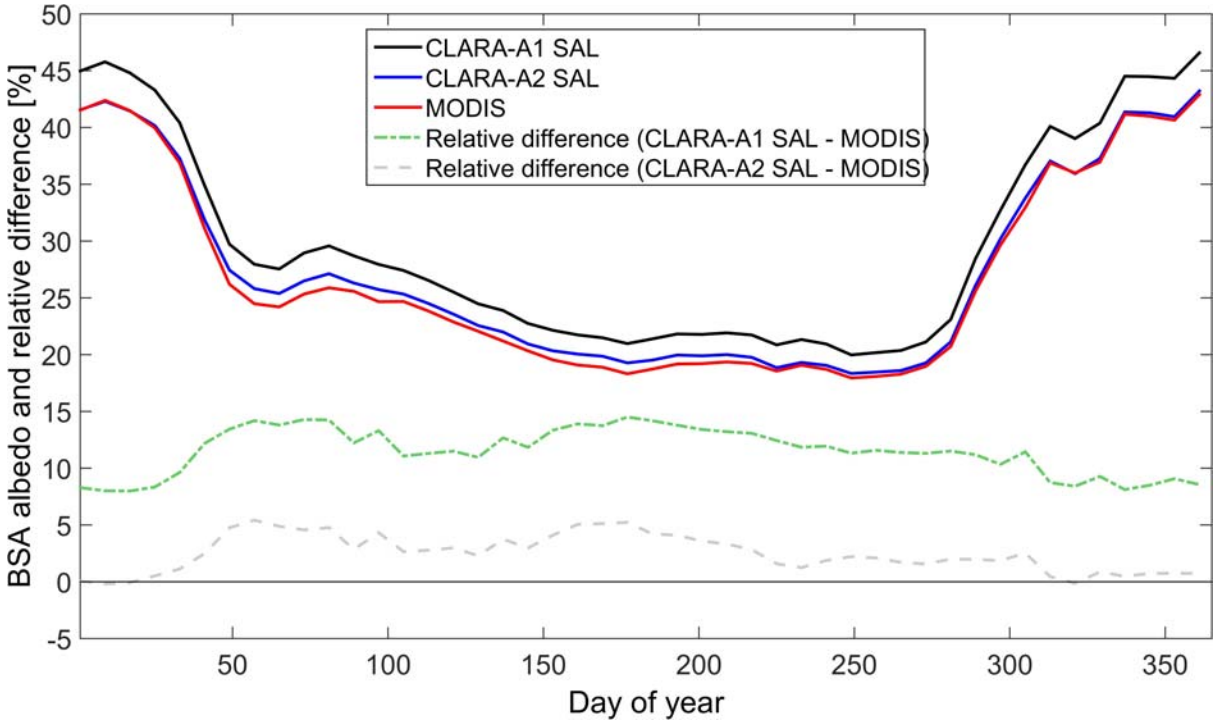

Figure 12: Comparison of surface albedos from CLARA-A2 SAL (blue line) and CLARA-A1 SAL (black line) pentad composites with MODIS MCD43C3 (red line) results for 2009 [unit is per cent]. The means are calculated only over those land/snow surfaces that are retrieved in both products, the MODIS product is not defined for water bodies, thus they are excluded from this analysis. No weighing for irradiance or area has been applied. The relative differences between the CLARA products and MCD43C3 are shown with a grey (CLARA-A2) and green (CLARA-A1) dash-dotted line.

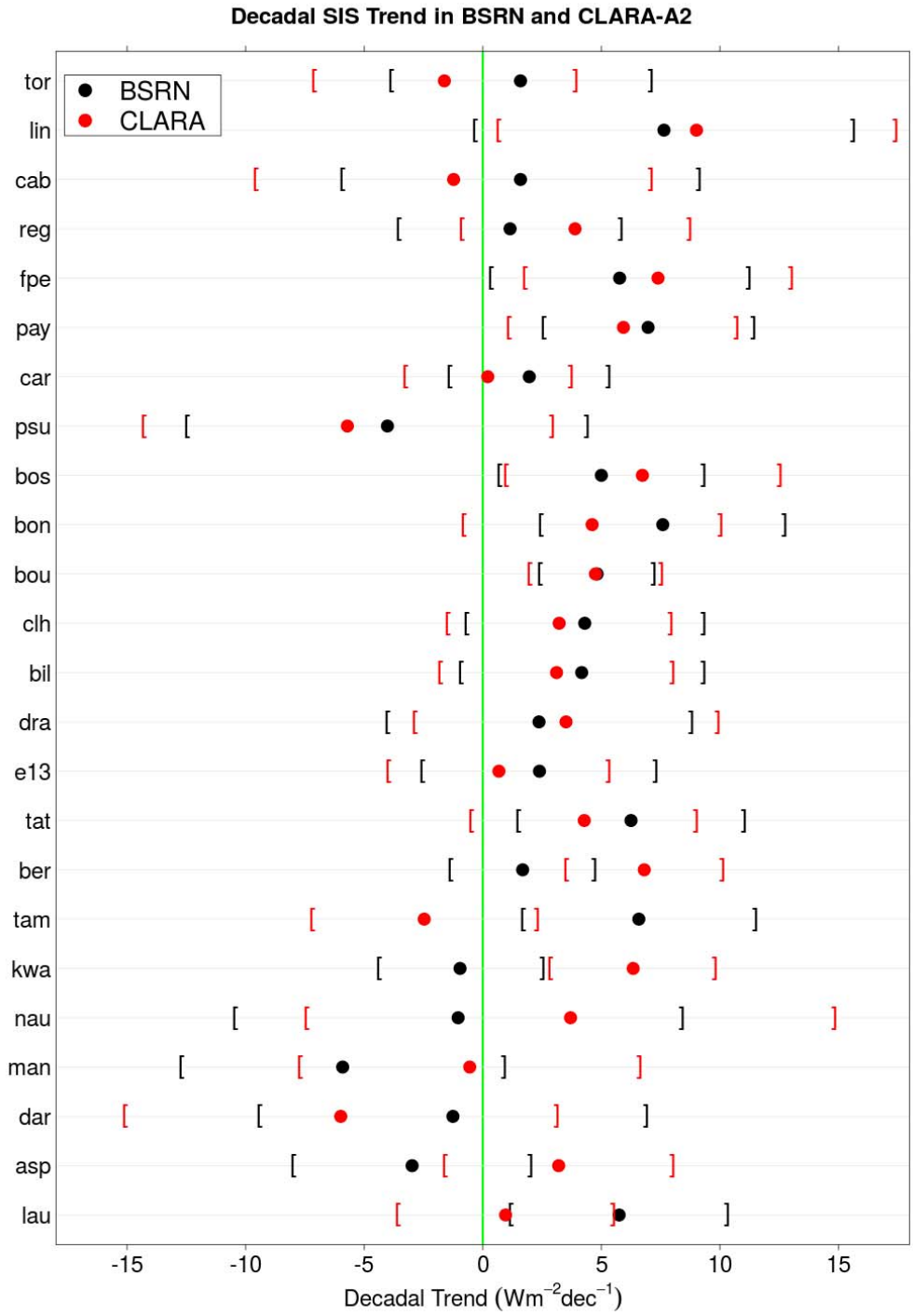

Figure 13: Decadal linear trends derived from the CLARA-A2 surface irradiance data record (red dots) with the corresponding trends derived from measurements obtained from the BSRN (black dots). Trends are shown as W m^{-2} (dec)$^{-1}$. The parentheses represent the confidence interval of the trends. See text for further details.

a)

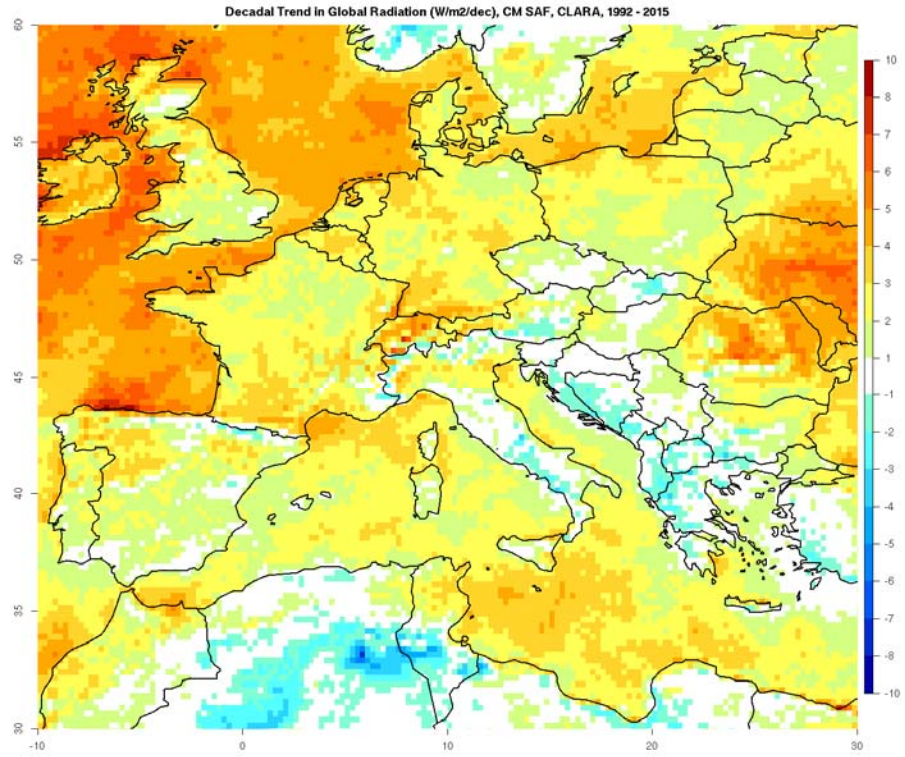

b)

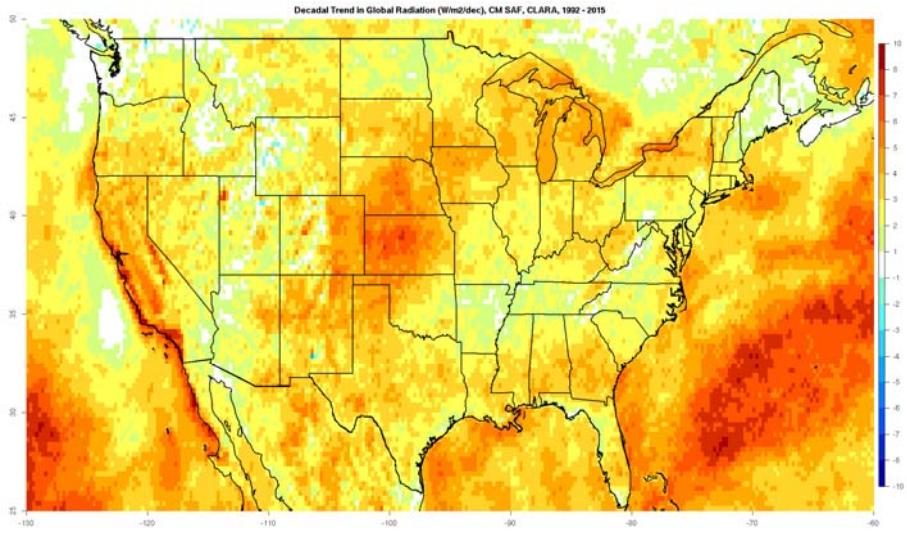

Figure 14: Decadal linear trend of the surface irradiance from 1992 to 2015 based on the CLARA-A2 SIS data record in (a) Central Europe and (b) parts of Northern America. All trends shown as W m^{-2} $(dec)^{-1}$.

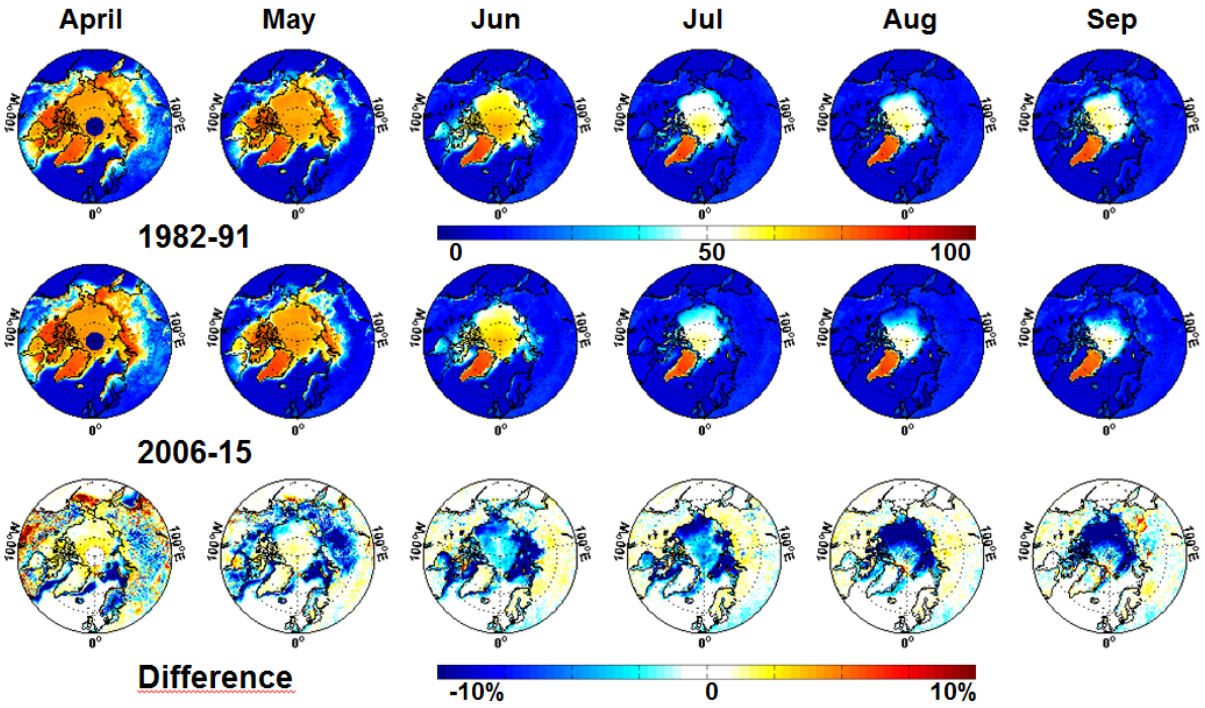

Figure 15: Arctic summer season mean surface albedo for the first CLARA-A2 decade (1982-1991, upper panel) compared to the last decade (2006-2015, middle panel). Difference plot (last minus first decade) shown in the lower panel. All values shown as %.

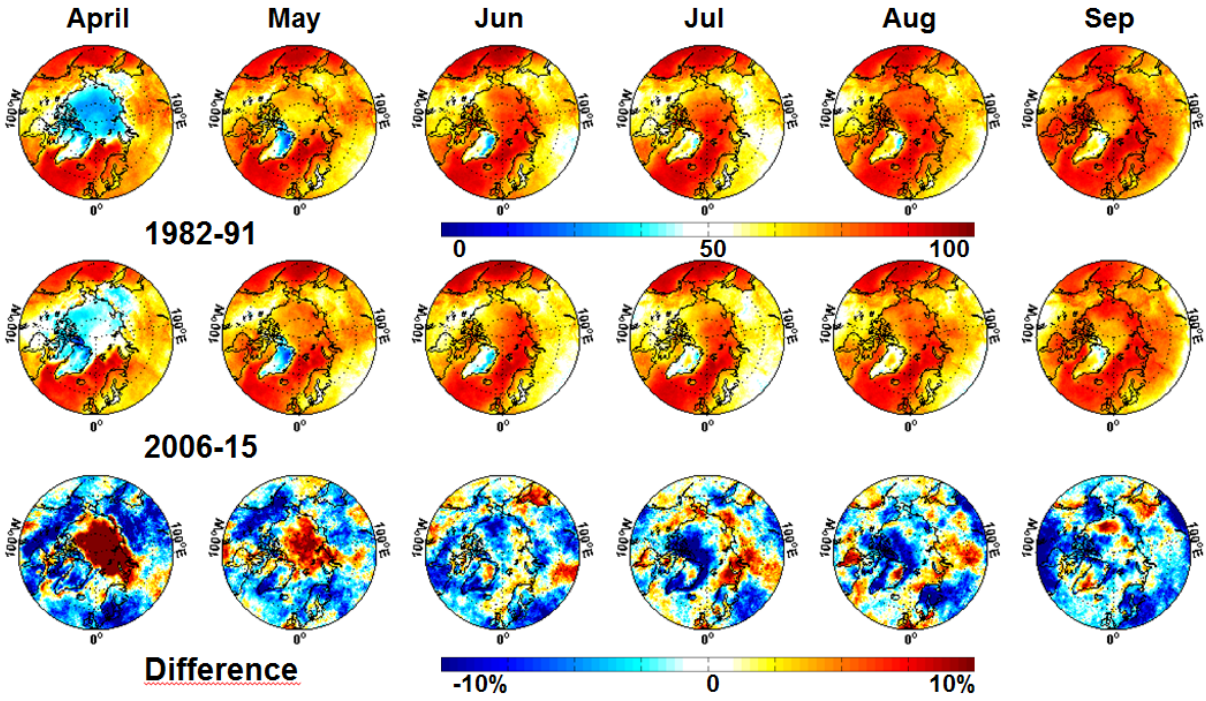

Figure 16: Arctic summer season mean cloudiness for the first CLARA-A2 decade (1982-1991, upper panel) compared to the last decade (2006-2015, middle panel). Difference plot (last minus first decade) shown in the lower panel. All values shown as %.

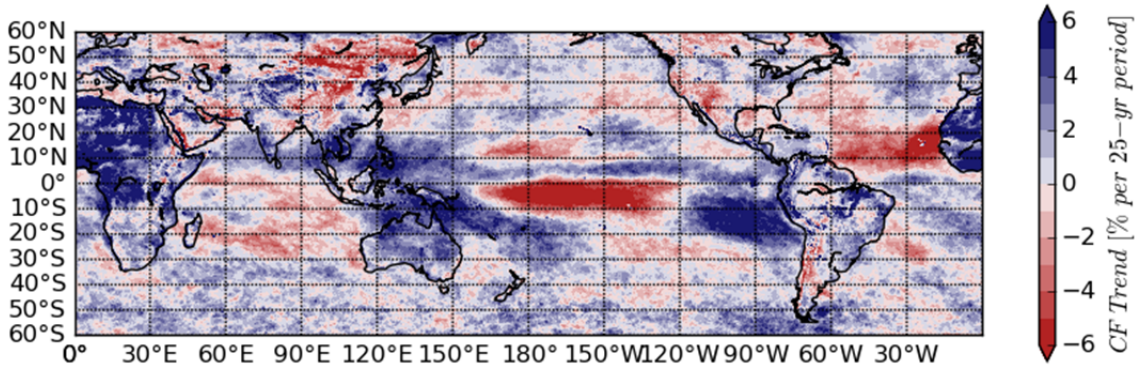

Figure 17: Average 25-year trend in cloud cover (%) for low and middle latitudes calculated on the basis of the average annual trend from CLARA-A2 in the period 1982-2015.